Preliminary Design of a Propellant Feed System for the μSTAMPS Thruster

A Thesis Presented for the

Master of Science

Degree

The University of Tennessee, Knoxville

Jack Stickley

August 2025

© by Jack Stickley, 2025
All Rights Reserved.

I dedicate this to my parents, for they have shaped me into who I am today, pushing me to continue getting better each day

Acknowledgments

I would like to thank Dr. Trevor Moeller for his continued guidance, mentorship, and dedication to an environment built for learning new things. Further, I would like to thank Dr. Brian Canfield and Alexander Terekhov for their assistance and guidance with this project, which was paramount to its success. Moreover, Brandon Meadows and Christian Sharpe for their aid, for without it, this project would not have had its success. I would also like to thank everyone at UTSI for making my time here enjoyable, as well as pushing me to be a better engineer and person. The varying perspectives provided to me on any range of topics will forever make me not only a better engineer, but a better person.

Abstract

CubeSats offer a low-cost, modular platform for space missions, but their capabilities remain constrained by limited propulsion options. The μSTAMPS micro-thruster, a compact electrospray propulsion device designed for CubeSats, is further limited in operational constraints by its minimal internal propellant reservoir. To overcome this limitation, a scalable and autonomous Propellant Feed System (PFS) has been developed to extend mission lifetimes and support more ambitious maneuvers. The PFS features a capacitance-based sensor for real-time fluid-level monitoring and an Arduino-based control circuit to autonomously regulate propellant delivery. Experimental validation confirmed accurate sensing, reliable pump functionality, and effective autonomous control. Challenges such as fluid routing complexity and minor electrical inconsistencies were addressed through iterative refinement. This work demonstrates a key advancement toward long-duration, self-regulating propulsion systems suitable for future CubeSat applications.

Table of Contents

1 Introduction **1**

1.1 CubeSats . . . 1

1.1.1 History of CubeSats . . . 3

1.1.2 Technological Evolution and Impact . . . 4

1.1.3 Challenges and Future Directions . . . 4

1.2 μSTAMPS . . . 6

1.3 Problem Statement . . . 11

1.4 Objectives . . . 12

1.5 Overview . . . 14

2 Literature Review **15**

2.1 CubeSat Propulsion Systems . . . 15

2.2 Fluid Level Sensing Techniques . . . 19

2.2.1 Capacitance-Based Sensors . . . 19

2.2.2 Conductivity Sensors . . . 20

2.2.3 Optical and Fiber-Optic Sensors . . . 20

2.2.4 Ultrasonic Sensors . . . 20

2.2.5 Thermal and Pressure-Based Methods . . . 21

2.2.6 Radio-Frequency (RF) Sensors . . . 21

2.2.7 Comparative Overview . . . 21

2.3 Control and Monitoring . . . 22

2.3.1 Pressure and Flow Regulation Mechanisms . . . 22

2.3.2 Integration and Control Implementation Strategies . . . 23

2.3.3 Microfluidic vs. Traditional Feed System Considerations 23
2.4 Key Gaps and Relevance 24

3 Methodology and Design Approach **25**
3.1 Sensor Selection and Characterization 25
3.2 Software Development, System Control, and Circuit Design 27
3.3 Model Development, Fluid Routing, and Considerations 28

4 Results and Discussion **30**
4.1 Subsystem Test Results 30
4.1.1 Sensor Validation 30
4.1.2 Fluid Flow Validation 32
4.1.3 LabVIEW and Circuit Control 38
4.2 Integrated System Performance 43
4.3 Successes and Limitations 48

5 Conclusion and Future Work **50**
5.1 Conclusions 50
5.2 Future Work 51

Bibliography **53**

Appendices **59**
A Full Calibration Sheet 60
B Pump Specification Sheet 61

Vita **62**

List of Tables

2.1 List of Companies and Their Electrospray Thrusters [3]. 18

4.1 Calibration of Capacitance Sensor provided by the manufacturer. 31

4.2 Specifications and values of the pump given by the manufacturer. 35

4.3 Peristaltic Pump tests at 3 V and 40 mA using a 60mL syringe. 36

List of Figures

1.1 Visual display of sizes of the CubeSat family, where 1U is the $10 \times 10 \times 10$ cm measure [2]. 2
1.2 Total CubeSats launched or scheduled to launch as of April 30, 2025 [4]. . . 5
1.3 μSTAMPS conceptual assembly schematic [5]. 7
1.4 Depiction of how electrospray technologies work. 7
1.5 Emitter types for electrospray propulsion [5]. 9
1.6 Depiction of the capillary to emitter chip design [5]. 9
1.7 Figure showing delta-v (Δv) requirements for changes in altitude or CAMs [6]. 10
1.8 Propellant required for each delta-v (Δv) maneuver for 3U and 6U CubeSats [5]. 12
1.9 Depiction of NASA's TRL and descriptions. 13

2.1 Figure showing the types of propulsion technologies used for CubeSats [12]. . 16
2.2 Thrust to power plots for electric propulsion technologies [3]. 16
2.3 Thrust vs specific impulse plots for electric propulsion technologies [3]. . . . 16
2.4 Diagram showing power vs specific impulse for varying electric propulsion types [3]. 17
2.5 Schematic of flight-like iodine propellant feed system [13]. 18

3.1 View of the test setup for the conductivity sensor. 26
3.2 Image of the scale reading for the mass of salt used in the 25 mL solution. . 29

4.1 Image showing the required wiring setup for the sensor's operation. 31
4.2 Image of the power supply used for the sensor, showing all power requirements. 32

4.3 Graph showing the calibration data for 0 - 3 mm fitted to a linear function and the fit equation. . . . 33
4.4 Graph showing the "super calibration"for the 0.6 - 2.4 mm range. . . . 33
4.5 View of model assembly showing the slot at the lower right for the sensor. . 34
4.6 Diagram of the sensor's design per the manufacturer. . . . 36
4.7 Interior view of the funnel model. . . . 36
4.8 View showing the ramp in the funnel, moving liquid from over the sensor into the disc. . . . 37
4.9 View of the side-entry model created, showing the through-hole for the tube placement. . . . 37
4.10 Depiction of the test setup with the side-entry model with syringe and pump. 37
4.11 Depiction of the test setup without the sensor secured. . . . 38
4.12 LabVIEW diagram showing the visual interface. . . . 39
4.13 LabVIEW wiring diagram for the tested VI for the True case (run pump). . 39
4.14 View of the false case (pump off) in the LabVIEW wiring diagram. . . . 40
4.15 Developed circuit schematic from TinkerCad. . . . 40
4.16 Depiction of the conceptual creation of the circuit in TinkerCad. . . . 40
4.17 View of the physical circuit setup. . . . 41
4.18 Part 1 of the Arduino code used, should be split into subplots to include them both. . . . 41
4.19 Continuation of the Arduino code used, from Fig. 4.18. . . . 42
4.20 View of the full setup used for testing. . . . 44
4.21 View of the electronics setup/wiring for testing. . . . 44
4.22 Image of the sensor fitted and secured into its slot. . . . 45
4.23 View of the sensors Integrated Circuit board with wiring. . . . 45
4.24 Image of a dry disc and inside, with a wet top post fluid-routing-test. . . . 46
4.25 View of the full internal reservoir post-test. . . . 46
4.26 View of the full internal reservoir post test with the sensor present at the top. 47

A.1 Calibration sheet provided by the manufacturer . . . 60

B.1 Specification Sheet for the pump 61

Chapter 1

Introduction

1.1 CubeSats

CubeSats, originally developed as a cost-effective platform for educational purposes, have evolved into versatile tools for space research and commercial applications [1]. They typically adhere to a standard size of $10 \times 10 \times 10$ cm or $(10 \text{ cm})^3$, referred to as "1U", with additional configurations available seen in Fig. 1.1 (e.g., 2U, 3U, 6U) to accommodate more sophisticated instruments and payloads [2]. These satellites weigh between 1 and 10 kg, and their compact design enables them to be launched as secondary payloads on rockets, reducing the cost of deployment [3]. CubeSats operate in low Earth orbit (LEO), between 160 to 2,000 kilometers above the Earth's surface, but some have ventured further into deep space [3]. The modularity of CubeSats allows for diverse applications, from Earth observation and weather monitoring to telecommunications and scientific research. Advances in miniaturized sensors have further enhanced their use in Earth observation, enabling high-resolution imagery for climate monitoring, disaster response, and agricultural assessments [1].

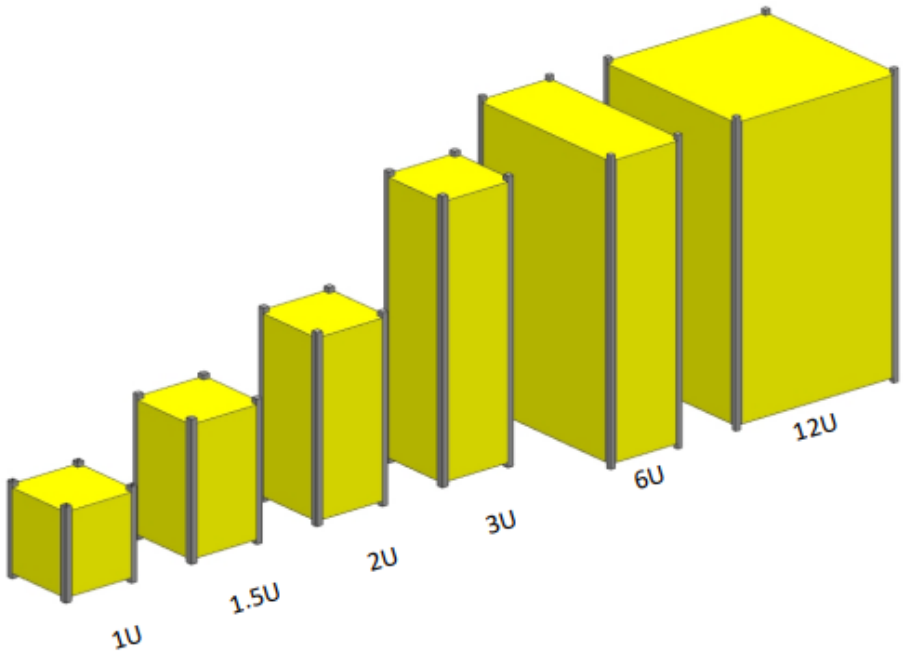


Figure 1.1: Visual display of sizes of the CubeSat family, where 1U is the $10 \times 10 \times 10$ cm measure [2].

The CubeSat's standardized form factor and commercial off-the-shelf (COTS) components make them an attractive option for universities, startups, and research institutions. They provide an affordable and accessible platform for technology demonstration and scientific experimentation, allowing for rapid iteration and innovation in satellite design[1, 2]. Moreover, the NewSpace industry, characterized by the increasing commercialization of space exploration and services, has adopted CubeSats to develop constellations for global internet coverage and space-based services. Despite their advantages, CubeSats face limitations, particularly in power generation, propulsion, and communication capabilities, due to their small size. To address these challenges, innovations in solar panel efficiency, deployable structures, and propulsion systems are being developed [3]. CubeSats are now pushing beyond LEO, with missions like NASA's "MarCO"(Mars Cube One), which successfully accompanied the InSight lander to Mars, showcasing the feasibility of small-scale satellites in interplanetary missions[3].

CubeSats are transforming the space industry by democratizing access to space and enabling low-cost innovation across scientific, commercial, and governmental sectors. Their continued evolution is expected to play a key role in space exploration, satellite communication networks, and Earth observation systems [1, 2].

1.1.1 History of CubeSats

The history of CubeSats began in 1994 when professors Jordi Puig-Suari from California Polytechnic State University and Bob Twiggs from Stanford University developed the concept as a low-cost, standardized satellite platform for educational purposes [1]. Their goal was to provide students with hands-on experience in satellite development while making space more accessible to academic institutions. The $(10\ \text{cm})^3$ "1U"CubeSat design, with a mass limit of 1.33 kg (for 1U), quickly became the standard. Early CubeSat missions were primarily launched as secondary payloads on rockets, piggybacking on larger satellite missions [2]. The first CubeSat launch occurred in 2003, marking the beginning of their operational history. This milestone demonstrated the viability of small satellites as practical tools for research and paved the way for subsequent innovations. Initially, CubeSats

were mainly used for educational purposes, technology demonstrations, and basic scientific experiments, but their potential for commercial applications soon became evident [3].

1.1.2 Technological Evolution and Impact

CubeSats have experienced significant growth over the past two decades, as seen by Fig. 1.2, driven by advancements in miniaturized technology, reduced launch costs, and increased demand for space-based data. The rise of commercial space companies like SpaceX, with their reusable rockets, has further reduced the cost of launching CubeSats. This has opened the door for a wide range of applications, including Earth observation, telecommunications, and even deep space missions. For example, the success of the Mars Cube One (MarCo) mission [3], which relayed critical data during the InSight lander's entry and descent on Mars, underscored the expanding role of CubeSats beyond Earth orbit and into interplanetary exploration. This milestone highlighted how small satellite platforms can provide valuable support for larger missions, paving the way for future deep space CubeSat applications. Simultaneously, CubeSat constellations are being leveraged to support global initiatives such as expanding internet access in underserved areas. the market has matured beyond academic roots, now encompassing startups, government bodies, and commercial ventures, all contributing to a dynamic and rapidly evolving "NewSpace"landscape.

1.1.3 Challenges and Future Directions

Despite their success, CubeSats face several limitations. Due to their small size, they have limited power generation capabilities, which restricts the types of instruments and sensors they can carry [3]. Communication bandwidth is also constrained, making it challenging to transmit large amounts of data to Earth. Additionally, CubeSats typically lack propulsion systems, limiting their ability to maneuver in space or extend their operational lifespan. While their modular design is a strength, it also imposes constraints on the payload size and complexity [2].

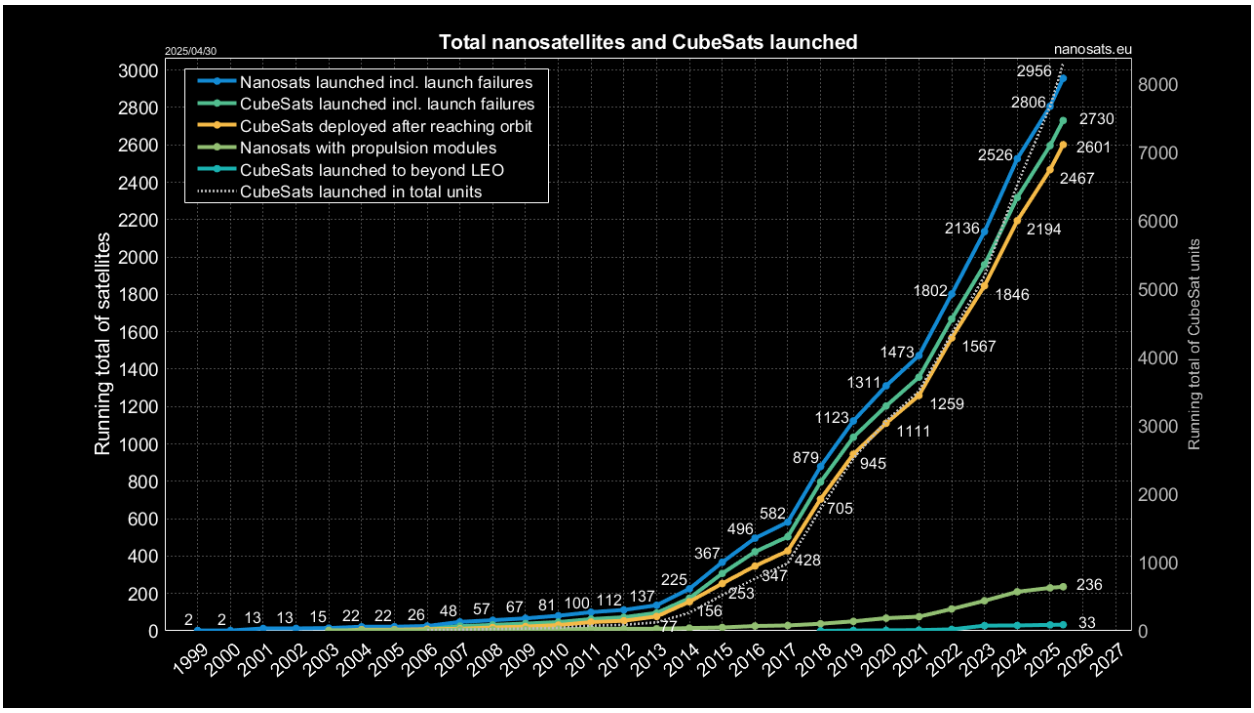


Figure 1.2: Total CubeSats launched or scheduled to launch as of April 30, 2025 [4].

Another challenge is the increasing congestion in low Earth orbit (LEO), where many CubeSats operate, raising concerns about space debris and the potential for collisions [3]. To address these challenges, innovations such as ion thrusters for propulsion, deployable antennas for communication, and de-orbiting technologies are being explored. There is also growing emphasis on ensuring CubeSats safely re-enter the atmosphere at the end of their mission life, reducing the risk of contributing to space debris [3].

CubeSats represent a major shift in the space industry by democratizing access to space and fostering rapid innovation. However, overcoming their inherent limitations will be crucial as they take on more complex and demanding missions, particularly in areas such as deep space exploration, long-term Earth observation, and satellite communication networks. Ultimately, it is this lack of propulsion that is a major issue. Given the described limitations, means of propulsion are limited by its available types of propulsion for its size, mass, and power constraints. While these options are limited, as CubeSats gain popularity, so is the desire to create means of propulsion for them. To solve this problem, many groups have dedicated time to creating solutions for this problem, innovating solutions for micro-propulsion technologies.

1.2 μSTAMPS

Micro Scalable Thrusters for Adaptive Mission Profiles in Space (μSTAMPS) represent a generational electric micro-propulsion technology developed at the University of Tennessee Space Institute (UTSI) aimed specifically at enhancing the capabilities of CubeSat missions by means of propulsion. A schematic of the assembly of the conceptual design can be seen in Fig. 1.3. These electric propulsion systems utilize the electrospray phenomenon, where ionic liquids (ILs), salts that are liquid at temperatures below 100 °C, are electrostatically extracted and accelerated to produce thrust (an example of this can be seen in Fig. 1.4), offering significant advantages in micro-propulsion including higher specific impulse, scalability, and precision thrust control crucial for station-keeping, collision avoidance, and de-orbit maneuvers in CubeSat platforms [5, 6].

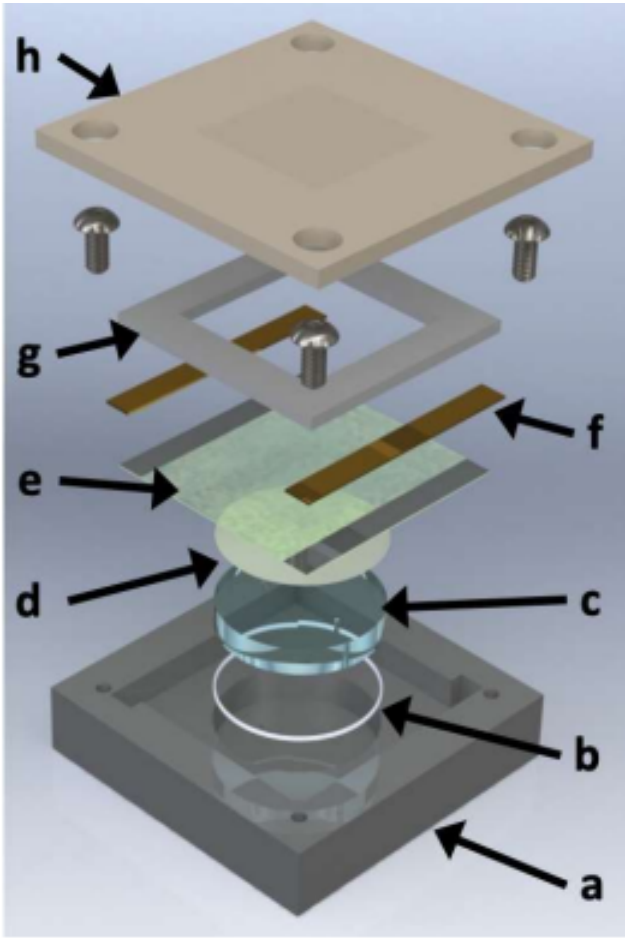


Figure 1.3: μSTAMPS conceptual assembly schematic [5].

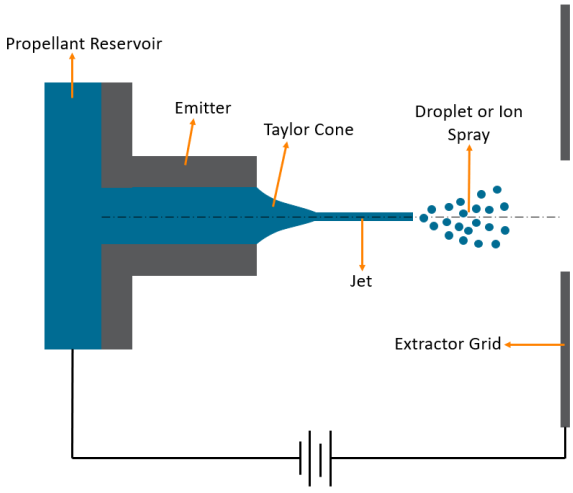


Figure 1.4: Depiction of how electrospray technologies work.

The μSTAMPS thruster employs a novel design, distinct from traditional electrospray emitters, seen in Fig. 1.5. It incorporates arrays of micro-capillary channels (approximately 1 μm in diameter and 170 μm in length), seen in Fig. 1.6, micro-machined into borosilicate glass using advanced ultra-fast laser techniques [5, 7]. This approach, involving Bessel-beam laser pulses, ensures precise control over the emitter geometry, critical for achieving reduced onset voltages and improved thruster robustness [8]. An integrated indium tin oxide (ITO) conductive coating acts as the extraction grid, further simplifying the thruster architecture by eliminating the need for external electrode alignment, reducing potential failure modes such as grid misalignment, mechanical damage, and propellant flooding [5, 9].

One of the primary innovations in μSTAMPS technology is its significantly lower electrospray onset voltage, optimized through detailed electrostatic simulations performed in ANSYS Electronics Desktop software by Jones et al. [10]. Typical state-of-the-art electrospray thrusters typically operate above 1 kV, posing risks for electromagnetic interference with other spacecraft components. Conversely, μSTAMPS emitters are designed to initiate electrospray at voltages as low as approximately 200 V, reducing complexity in spacecraft integration and potential interference risks.

μSTAMPS thrusters demonstrate capabilities for station-keeping, collision avoidance, and rapid de-orbit maneuvers for nanosatellites in Low Earth Orbit (LEO). A trade study simulation using FreeFlyer software [11] has shown that μSTAMPS thrusters can effectively maintain the orbit of 3U and 6U CubeSats at altitudes between 300 km and 600 km over a typical mission duration of five years, consuming minimal propellant [6]. For collision avoidance maneuvers (Δv ranging from 0.3 to 1 m/s, seen in Fig.1.7), the system proved capable of maneuvers within hours, considerably faster than the two-day advance collision notice required by typical operational scenarios such as those used by the International Space Station (ISS). This demonstrates the system's suitability for responsive orbital maneuvering and efficient mission operations.

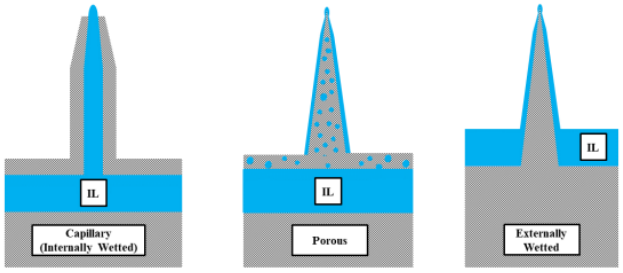


Figure 1.5: Emitter types for electrospray propulsion [5].

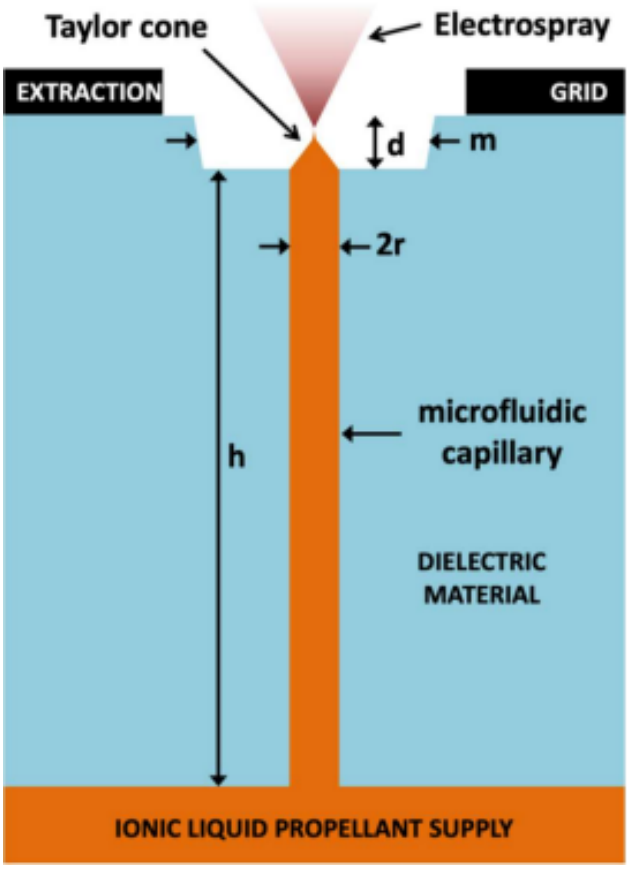


Figure 1.6: Depiction of the capillary to emitter chip design [5].

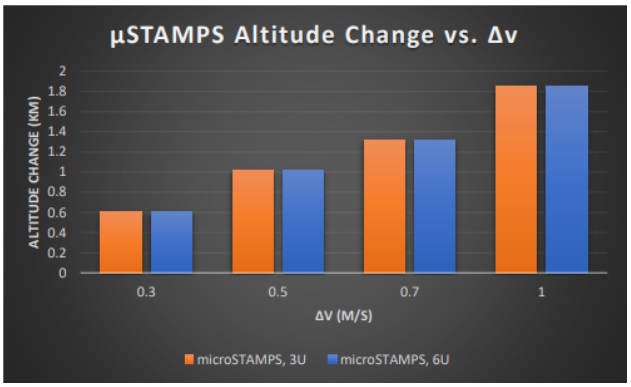


Figure 1.7: Figure showing delta-v (Δv) requirements for changes in altitude or CAMs [6].

Further experimental validation performed under vacuum conditions at UTSI demonstrated successful operation of μSTAMPS using non-stoichiometric hydroxyethyl hydrazinium nitrate (NSHEHN) IL propellant (it should be noted that further study has shown the use of butyl methylpyrrolidinium dicyanamide (BMP-DCA) to be a much better option for an IL). Electrospray onset voltages were recorded as low as 1300 V with measurable electrospray currents on the order of 0.1 μA [7]. The performance metrics calculated from these tests estimated thrust levels in the 1-10 μN range and thrust densities on the order of 0.001 N/m^3, indicating that the μSTAMPS thruster is capable of meeting and potentially surpassing mission requirements for CubeSat propulsion. (It should be noted that this work was very preliminary and more work is being done to verify more on this.)

The fabrication approach employed to construct μSTAMPS thruster chips involves two principal steps using ultra-fast laser micro-machining, initial formation of micro-capillaries followed by the excavation of electrospray cavities via water-assisted cavitation [5, 8]. The current fabrication methods show high repeatability, producing emitter arrays rapidly and reliably at rates on the order of 1000 capillaries per second, paving the way for future mass production and rapid integration into CubeSat platforms. Ongoing development aims to transition to thicker cover slips for greater mechanical robustness and optimization of electrospray onset voltages, as well as exploring surface treatment methods to enhance propellant flow control and operational reliability [7, 9]. Future methods of fabrication methods will most likely employ UV ablation, providing a better and faster option.

The thruster presents a promising advance in micro-propulsion technology, providing critical capabilities for orbit maintenance, precise maneuvering, and rapid, controlled de-orbiting of CubeSats. Continued research and testing at UTSI promise to further this technology, positioning μSTAMPS as a robust, efficient propulsion solution tailored specifically for next-generation small spacecraft missions [5].

1.3 Problem Statement

The advancement of micro-propulsion systems, particularly electrospray thrusters such as μSTAMPS, presents substantial opportunities for enhancing the capabilities of CubeSats and other nanosatellites. However, the current state of these propulsion systems face significant limitations primarily due to their restricted propellant capacities, hindering their operational endurance and maneuvering capability. The current iteration of the μSTAMPS thruster, while offering considerable promise with high specific impulse and precise thrust control, inherently accommodates only 0.2 g of IL propellant within its integrated porous reservoir, severely limiting mission scope in duration. Fig. 1.8 shows the propellant requirements, demonstrating the need to provide propellant beyond the current.

Consequently, there exists a critical need for an improved and scalable external propellant feed system capable of significantly increasing propellant storage capacity, targeting a storage capacity of up to 100 g, to enable extended mission durations and complex operational profiles such as prolonged station-keeping, repeated collision avoidance maneuvers, and rapid de-orbit capabilities. Addressing this challenge requires the development of a robust, efficient, and scalable Propellant Feed System (PFS) capable of reliably managing larger propellant volumes within the stringent constraints posed by small satellite platforms. Essential considerations in the design include effective fluid routing, pump integration, accurate fluid-level monitoring, and maintaining strict compatibility with vacuum and potential cryogenic environments.

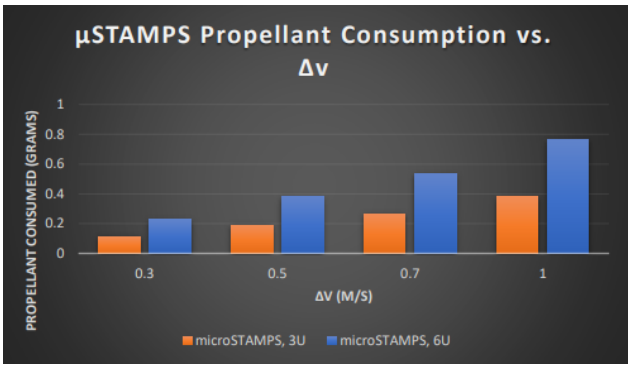


Figure 1.8: Propellant required for each delta-v (Δv) maneuver for 3U and 6U CubeSats [5].

This project aims to address these challenges through the design, fabrication, and testing of a preliminary propellant feed system capable of delivering enhanced propellant volumes up to 100 g to the μSTAMPS, thereby substantially improving the thruster's mission capabilities. The project emphasizes modularity, ease of modification, and scalability, laying foundational groundwork for subsequent developmental phases toward space-readiness. Success in developing such a propellant feed system will significantly enhance the functional utility of CubeSat platforms by providing extended mission durations, improved operational flexibility, and increases capability for complex maneuvers and mission profiles.

1.4 Objectives

The primary objective of this project is to develop a preliminary Propellant Feed System (PFS) for the μSTAMPS micro-thruster that meets essential performance requirements for CubeSat applications while laying the groundwork for future design iterations. In this early phase, targeting a NASA Technology Readiness Level (TRL) 4 (seen in Fig. 1.9), which emphasizes component and breadboard validation in a laboratory environment; the system is envisioned as a working prototype that demonstrates autonomous propellant management through accurate fluid-level sensing, efficient fluid routing, and robust control via an embedded circuit/micro-controller.

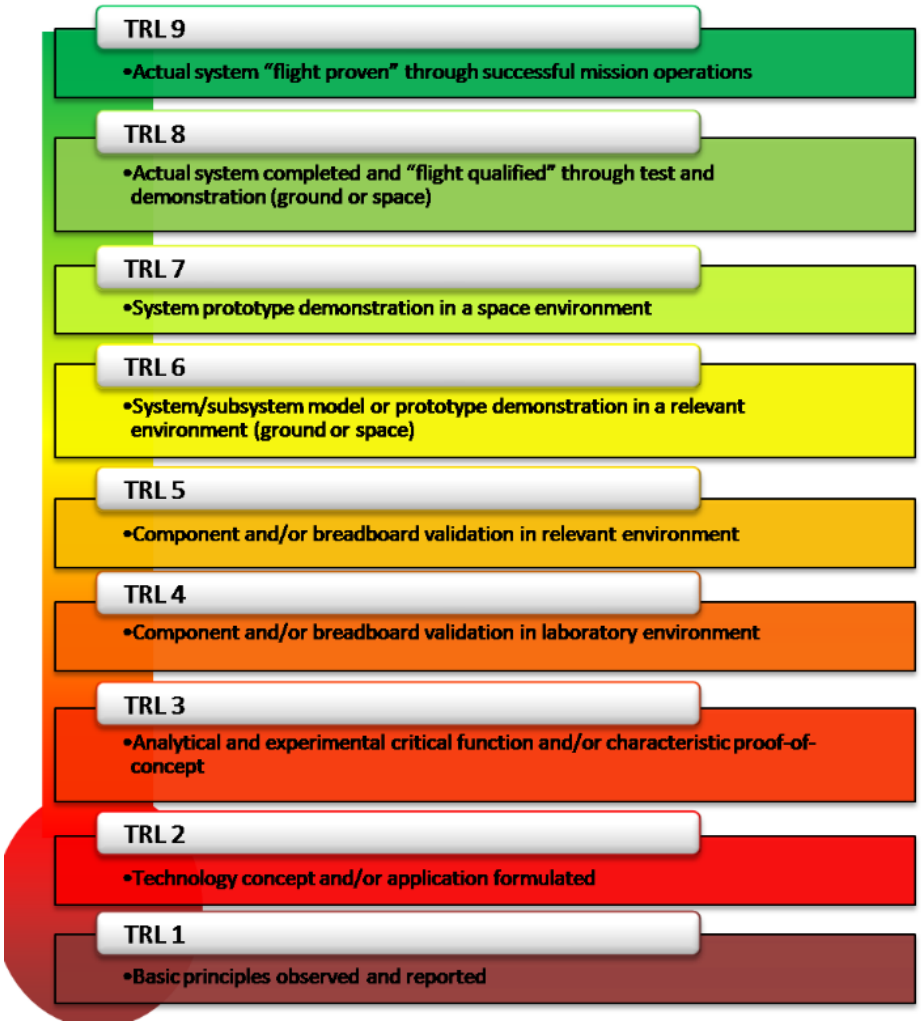


Figure 1.9: Depiction of NASA's TRL and descriptions.

To this end, the design will focus on defining clear system requirements, and interface controls, mitigating risks associated with power consumption and mass constraints, and incorporating a user-friendly control interface that promotes self-sufficiency by minimizing external dependencies. The objectives include establishing a reliable sensor mechanism to monitor propellant levels within a compact reservoir, integrating this sensor with a pump and control circuitry, and ensuring that the overall system architecture can be readily modified and scaled to meet the more demanding conditions anticipated at higher TRL stages, such as TRL 5, where validation occurs in a relevant environment. These steps are critical for transitioning from a preliminary design to a final, flight-ready system by addressing fundamental systems engineering factors –such as design scalability, interface management, and iterative risk mitigation, that are essential for the successful deployment of micro-propulsion technologies in space.

1.5 Overview

The outline of this thesis presents the research and development activities aimed at creating a scalable and autonomous Propellant Feed System (PFS) tailored for the μSTAMPS thruster, specifically for enhancing CubeSat propulsion capabilities. Chapter 2 offers a comprehensive literature review covering CubeSat propulsion technologies, fluid-level sensing techniques in space, and control mechanisms, highlighting existing gaps or useful technologies and defining the necessity for improved propellant management systems. Chapter 3 outlines the methodological approach, detailing sensor selection, calibration, circuit and software development, and iterative design processes for fluid routing models. Chapter 4 discusses the results from subsystem validations, integrated system performance, and identifies successes alongside areas for improvement. Finally, Chapter 5 summarizes the conclusions drawn from the project and outlines recommendations for future enhancements, including the miniaturization of electronics, development of robust system housing, optimization of the fluid routing, and alternative methodologies to further improve the reliability and operational efficiency of the propellant delivery system.

Chapter 2

Literature Review

2.1 CubeSat Propulsion Systems

CubeSats, small-scale satellites typically weighing between 1 kg and 10 kg, have gained popularity due to their lower cost, rapid development cycles, and versatility in applications ranging from Earth observation to deep space exploration. A critical component in enhancing the operational capabilities of CubeSats is the integration of efficient propulsion systems capable of precise orbital maneuvers, station-keeping, and extending mission lifetimes.

General insights provided by Parker and Folta [12] outline foundational concepts and comparative insights across multiple propulsion strategies, emphasizing the critical balance between propulsion performance, CubeSat size constraints, and mission duration [12]. Propulsion methods broadly fall into chemical, cold gas, electric, and hybrid categories, each offering distinct advantages and limitations related to thrust magnitude, specific impulse (Isp), complexity, and scalability. Varying types of in-space propulsion that generalize these forms can be seen in Fig. 2.1, whereas their performance metrics can be seen in Figs. 2.2 and 2.3. Chemical propulsion, typically involving liquid or solid propellants, provides high thrust but suffers from limited scalability and higher system mass. Cold gas systems, meanwhile, offer simplicity and reliability but at the expense of relatively low performance metrics. In contrast, electric propulsion methods, including Hall-effect thrusters and electrospray systems, offer superior specific impulse, efficiency, and precise maneuverability suitable for

extended CubeSat missions. Their general metrics can be seen in the power vs specific impulse plot, seen in Fig.2.4.

System Type	Product	Thrust	Specific Impulse (s)	TRL Status
CHEMICAL	Hydrazine	0.5 – 30.7 N	200-235	9
	Cold Gas	10 mN – 10 N	40 – 70	GN2/Butane/R236fa 9
	Alternative (Green) Propulsion	0.1 – 27 N	190 – 250	HAN 6, ADN 9
ELECTRIC	Pulsed Plasma and Vacuum Arc Thrusters	1 – 1300 μN	500 – 3000	Teflon 7, Titanium 7
	Electrospray Propulsion	10 – 120 μN	500 – 5000	7
	Hall Effect Thrusters	10 – 50 mN	1000 – 2000	Xenon 7, Iodine 3
	Ion Engines	1 – 10 mN	1000 – 3500	Xenon7, Iodine 4
PROPELLANTLESS	Solar Sails	0.25 – 0.6 mN	N/A	6 (85 m²), 7 (35 m²)

Figure 2.1: Figure showing the types of propulsion technologies used for CubeSats [12].

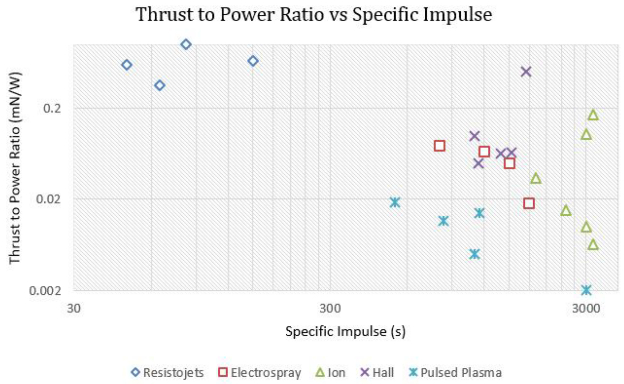


Figure 2.2: Thrust to power plots for electric propulsion technologies [3].

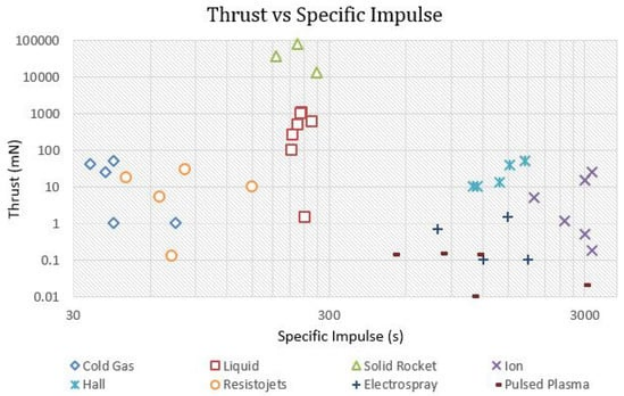


Figure 2.3: Thrust vs specific impulse plots for electric propulsion technologies [3].

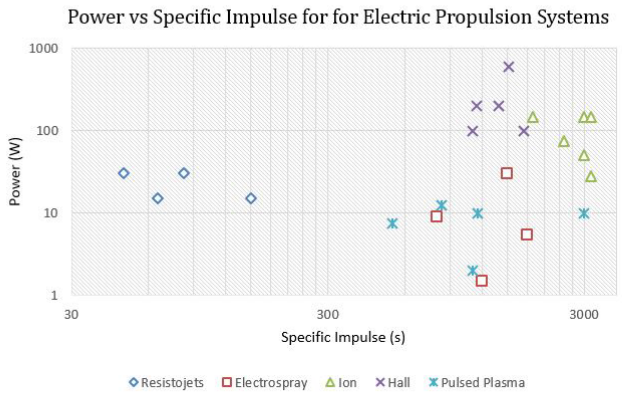


Figure 2.4: Diagram showing power vs specific impulse for varying electric propulsion types [3].

Electric propulsion technologies, particularly suited for CubeSat applications, have attracted significant research attention due to their high efficiency and relatively lower propellant requirements. Hall-effect thrusters, traditionally utilizing xenon as a propellant, have recently seen innovation with alternative propellants such as iodine, as evaluated by Polzin and Peeples [13]. Their research demonstrated iodine's advantages, including improved storage density and low ionization energy, making it particularly attractive for compact CubeSat missions. The schematic diagram provided in their work effectively demonstrates system integration opportunities, can be seen by Fig. 2.5 [13]).

Electrospray propulsion represents another major advancement within electric propulsion, offering precision control, scalability, and compact system integration. Some examples of work done on these systems can be shown by Table 2.1. Martinez and Mease confirmed electrospray thrusters' capability for precision maneuvers such as orbital corrections and constellation maintenance, highlighting the technology's effectiveness for mission-specific tasks metrics from [14]. Perna et al. expanded upon this by demonstrating successful autonomous attitude control of CubeSats using electrospray systems, further highlighting their suitability for missions with stringent power and control demands [15].

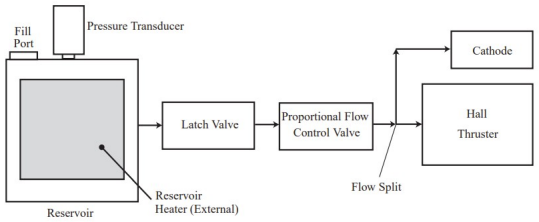


Figure 2.5: Schematic of flight-like iodine propellant feed system [13].

Table 2.1: List of Companies and Their Electrospray Thrusters [3].

Company/Institution with Location	Engine	Thrust (mN)	I_{sp} (s)	Power (W)	Propellant
MIT, Cambridge, MA, USA	S-iEPS	0.1	1200	1.5	ionic liquid
Accion Systems, Boston, MA, USA	TILE 5000	1.5	1800	30	ionic liquid
Busek, Natick, MA, USA	BET-1mN	0.7	800	<9	ionic liquid
Busek, Natick, MA, USA	BET-100	0.005–0.1	1800	5.5	ionic liquid

Additionally, Greig et al. have innovated structural integration by embedding electrospray thrusters directly into CubeSat rails, addressing volume constraints critical for small satellite designs [16]. Lenguito et al. further investigated multiplexed electrospray propulsion, showcasing its scalability potential and performance versatility in supporting various CubeSat mission scenarios [17].

Complementing technical evaluations, decision-making and trade-off analyses by Parker and Folta provide a robust framework for propulsion technology selection tailored to specific mission needs. Their decision analysis methodology presents an objective means of comparing different propulsion technologies, focusing on reliability, thrust performance, power consumption, and mass constraints [18].

A broader and comprehensive review by Alnaqbi et al. explores propulsion technologies extensively, analyzing multiple electric propulsion systems and emphasizing the advantages of compact designs and multiplexed configurations, which provide scalability and improved performance adaptability [19]. Complementing this, detailed work by Chiarot et al. investigates microfluidics applications of electrospray systems, demonstrating additional pathways for propulsion miniaturization and performance optimization within microscale systems [20]. Krejci et al. further present scalable electrospray designs adaptable to CubeSat missions of varying complexity, emphasizing adaptability to power and mass budgets [21].

Finally, critical reviews and comparisons conducted by O'Reilly et al. and Tummala and Dutta provide extensive overviews of electric propulsion systems. They underline the importance of evaluating propulsion systems based on mission-specific parameters and detail recent technological trends and improvements in propulsion strategies, particularly electric propulsion, confirming its suitability for most CubeSat applications requiring fine orbital adjustments and long-duration missions [22, 3].

2.2 Fluid Level Sensing Techniques

Measuring propellant levels in space is notoriously challenging due to microgravity. Unlike on Earth, where gravity pools liquid at the bottom of a tank, in orbit the fluid can float and cling to walls unpredictably [23]. This is especially problematic for micro-propulsion systems that carry limited fuel and operate in microgravity. Over the decades, various sensing techniques have been developed and tested to gauge fluid levels or mass in spacecraft tanks. Early satellites often relied on indirect methods or bookkeeping methods of fuel usage, but modern research has focused on sensor-based approaches that can directly measure remaining propellant in real-time. Major experimental and demonstrated techniques are reviewed such as: capacitance, conductivity, optical, ultrasonic, thermal, and radio-frequency methods; highlighting their historical development and recent advancements.

2.2.1 Capacitance-Based Sensors

Capacitive sensors exploit the difference in dielectric constant between liquid propellant and gas to infer liquid quantity. Capacitance-based sensing has been studied since the 1960s, including NASA's Apollo-era feasibility studies [24]. Capacitive sensors have become a common approach for settled propellant measurement; Meteosat satellites utilized Gauging Sensor Units (GSUs) based on capacitive principles, significantly improving end-of-life fuel estimates [25]. Modern Electrical Capacitance Tomography (ECT) systems provide detailed imaging of fluid distribution with high accuracy—often within 1% of total tank mass—even with fluid sloshing or unsettled conditions [24]. A notable example, smart tanks for space (SMARTTS) technology, employs ECT-based arrays to provide precise real-time propellant

mass measurement, with planned in-orbit demonstrations further proving its applicability [26].

2.2.2 Conductivity Sensors

Conductivity-based level sensors detect fluid presence using electrical conduction through the liquid, primarily suited for conductive propellants or water-based fluids [27]. Despite their simplicity, absence of moving parts, and ease of readout, these sensors are limited by their binary nature (wet/dry detection) and require fluid compatibility. Conductivity sensors also raise concerns of corrosion or electrochemical reactions and provide only discrete, rather than continuous, level information. Their usage in microgravity often demands specific design adaptations to ensure reliable fluid contact and signal clarity.

2.2.3 Optical and Fiber-Optic Sensors

Optical sensing leverages refractive index changes when fluid interfaces with sensor tips or fiber segments. Fiber-optic techniques, including distributed fiber sensing, have been developed by NASA and others to measure continuous propellant levels with sub-percent accuracy and millimeter spatial resolution [28]. Fiber-optic sensors offer immunity to electromagnetic interference, safety benefits (no electrical current in propellant), and capability for distributed, high-resolution sensing. Demonstrations have effectively measured cryogenic propellants, indicating their suitability for future micro-propulsion systems, although precise optical alignment and robust component design remain critical considerations.

2.2.4 Ultrasonic Sensors

Ultrasonic sensors use acoustic pulses to measure fluid presence and height, offering a non-intrusive and proven method extensively validated on spacecraft such as the Meteosat Second Generation satellites [25]. Ultrasonic sensors have achieved sub-percent accuracies and provided a reliable alternative to bookkeeping methods for end-of-life fuel estimation. However, they can be sensitive to temperature variations and fluid scattering effects, particularly if liquids form irregular configurations in microgravity. Continued refinement

and careful calibration have allowed ultrasonics to be a viable and trusted sensing technology in spacecraft propulsion tanks.

2.2.5 Thermal and Pressure-Based Methods

Thermal and pressure-based methods, including Pressure-Volume-Temperature (PVT) gauging, indirectly estimate fluid quantity using thermodynamic properties [29]. They are inherently simple but slow and rely on assumptions such as stable thermal equilibrium and uniform fluid distribution. Consequently, they generally serve as complementary checks, providing redundancy rather than standalone solutions, especially as accuracy significantly decreases as propellant volumes become minimal.

2.2.6 Radio-Frequency (RF) Sensors

Radio-frequency mass gauges (RFMG) use electromagnetic resonances to sense propellant mass distribution without relying on gravity-induced settling [23]. NASA's RFMG has demonstrated promising results in small-scale experiments aboard the ISS and parabolic flights, with a full-scale demonstration aboard a lunar lander scheduled for 2024. RFMG technology is advantageous due to its potential to measure bulk fluid mass in real-time, independent of fluid configuration, though complexities in calibration and interpretation require further validation through long-duration spaceflight demonstrations.

2.2.7 Comparative Overview

Each fluid level sensing method has unique strengths and limitations. Capacitance and ultrasonic sensors are highly reliable due to extensive spaceflight heritage and proven accuracy. Fiber-optic and RF sensors represent newer advancements, offering higher resolution and comprehensive measurement capabilities but are still undergoing rigorous space qualification. Conductivity, thermal, and pressure methods typically complement primary sensors, providing redundancy. Increasingly, combined sensor arrays or hybrid systems are proposed, merging real-time primary measurements with secondary confirmation techniques to enhance robustness, accuracy, and redundancy in future micro-propulsion

missions. Given the scope of cost and sizing of the CubeSat development, it could be determined that capacitance or conductive sensors would be optimal for the propellant feed system.

2.3 Control and Monitoring

Electrospray thrusters utilize electrostatic fields to accelerate charged droplets or ions from conductive IL propellants. They offer high specific impulse and precise thrust control, making them well-suited for CubeSats and other small satellite applications [30, 31]. Reliable and efficient propellant feed management is crucial for system performance, especially given the micro-scale flows typical of electrospray systems, which introduce unique challenges for propellant regulation and control [32].

2.3.1 Pressure and Flow Regulation Mechanisms

Passive, capillary-driven feed systems use surface tension and capillary forces to manage propellant flow without pumps or regulators. Notable examples include Busek's BET-300-P and MIT/Aerojet Rocketdyne's S-iEPS thruster, both of which utilize porous emitters to passively transport propellant [33, 34]. The inherent physics of electrospray emission naturally regulates propellant flow, significantly reducing complexity, mass, and the risk of mechanical failures [33, 35]. However, passive feed systems typically offer limited direct throttling capabilities, relying instead on adjustments in emitter voltage or the number of active emitters to modulate thrust [34].

Active propellant feed systems utilize a controlled pressure differential generated by inert gases or mechanical systems such as bladders or spring-driven reservoirs [8]. These systems facilitate precise control over propellant delivery, particularly beneficial for internally wetted emitter designs. Research by Galobardes-Esteban et al. demonstrated regulated systems operating at moderate pressures ($\sim$500 Torr), employing microvalves for precise flow control [35]. Such active systems typically incorporate electrically actuated valves designed for high-voltage isolation, minimal dead volume, and energy-efficient, low-power

operation [35]. Recent advancements include compact, 3D-printed microvalves that offer reliable performance, minimal leakage, and low power consumption [35].

Determining the necessity of pressure and flow regulation largely depends on mission objectives and thruster architecture. Passive systems significantly simplify design, reduce mass, and increase reliability, ideal for CubeSat applications with stringent mass constraints [35]. Conversely, active systems are advantageous when missions require precise thrust modulation, instantaneous shut-off capability, or robust operation under varying environmental conditions, despite their added complexity and mass [35, 35].

2.3.2 Integration and Control Implementation Strategies

Integration of control and monitoring into electrospray propulsion systems involves embedding sensors, actuators, and electronics into a compact, robust architecture suitable for CubeSat constraints. An effective integration strategy includes: high-voltage isolation [32], miniaturization [36], fault tolerance [31], and real-time telemetry and closed-loop control [31, 35]. Integrated control electronics typically communicate with the satellite's avionics through standardized interfaces. Micro-controller based Power Processing Units (PPU's) are commonly used for regulated voltage, emission current, actuating valves, and processing sensor data for autonomous adjustments and fault mitigation [36, 31]. Furthermore, bubble management and propellant priming protocols are essential, as gas bubbles significantly degrade electrospray stability. Proper priming and automated bubble management strategies, including valve cycling or voltage adjustments, ensure consistent, reliable propellant feed [35].

2.3.3 Microfluidic vs. Traditional Feed System Considerations

Microfluidic feed systems utilize miniature channels or integrated capillary networks to distribute propellant passively through capillary action. This approach inherently stabilizes flow, eliminates the need for active valves or regulators, and dramatically reduces complexity and mass, aligning closely with CubeSat requirements [36]. Notable examples

include MEMS-based thruster arrays, where micro-channels uniformly distribute propellant, significantly simplifying system architecture [34, 36].

Traditional feed systems, on the other hand, rely on external reservoirs, valves, and regulated pressurization. While more complex, they provide significant flexibility and precise control of flow rates, enabling active throttling and redundancy [35, 34]. Traditional systems, however, increase complexity, mass, and risk of failure, necessitating careful design and integration. In summary, microfluidic systems offer simplified architectures ideal for CubeSat missions prioritizing reliability and compactness, whereas traditional systems may better serve missions demanding precise active control despite increased complexity [35].

2.4 Key Gaps and Relevance

Given the novelty and recency of electrospray propulsion, the methodologies listed in this chapter pertaining to propellant feed systems must be explored; especially for a ground-breaking technology like the μSTAMPTS thruster. A key limitation of the current μSTAMPS design however, is in its propellant supply; it carries only a small amount of internal reservoir of IL, sufficient for brief collision avoidance maneuvers (CAMs), but lacks an external propellant feed system for longer duration or higher Δv missions. This absence of a feed system is a critical gap restraining μSTAMPS from reaching its full potential in CubeSat missions beyond basic maneuvers. Without an external feed mechanism, μSTAMPS is limited to the propellant contained in its tiny on-board reservoir, severely capping the total impulse (and Δv) available, shortening mission lifetime and constraining operational scope. Researchers at UTSI have identified a critical need for an improved and scalable propellant feed system to increase propellant storage (up to 100 g of IL) and enable extended mission profiles [6]. In other words, to perform advanced maneuvers, μSTAMPS must be equipped with a feed system that can store and deliver much more propellant than the internal reservoir alone [5]. This gap was previously explored by Tyler Sundstrom [37], through the creation of a tank and 3D printed microfluidic chips; however, such a feed system was deemed unsuccessful and further work was needed.

Chapter 3

Methodology and Design Approach

The methodology and design approach for the development of the preliminary propellant feed system (PFS) for the μSTAMPS thruster was strategically structured to address both technical and operational requirements inherent to CubeSat missions. The focus was to iteratively design, implement, and validate a functional PFS capable of delivering propellant from an external tank to the μSTAMPS thruster's internal reservoir, with minimal human interface (if any), while maintaining compact and cost-effective principles critical for CubeSat applications. The approach entailed several key phases: sensor selection and testing, control system and circuit design, software development for the system, physical model development for fluid routing, and full system integration and preliminary testing. Each incorporated iterative testing and analysis to ensure alignment with the primary goal: delivering a scalable and autonomous PFS suitable for μSTAMPS and possibly broader CubeSat platforms.

3.1 Sensor Selection and Characterization

The development process begins with identifying a suitable sensor to monitor fluid levels within the μSTAMPS disc reservoir. The initial selection focused on a conductivity sensor, selected due to the conductive nature of the ILs intended for use as propellant; its general test setup can be seen in Fig. 3.1. Although this sensor is simple and capable of detecting fluid presence, tests revealed its inability to provide continuous level measurements, instead

offering binary "wet/dry" data that is inadequate for precise control. As a result, further research into alternative sensing methods was conducted.

The Capacitec thin capacitance sensor was ultimately selected based on its compatibility with small-scale geometries and its ability to provide continuous fluid level measurements. The sensor is custom-calibrated by the manufacturer to a measurement range of approximately 0.6 mm to 2.4 mm, with a greater range of 0-3 mm, matching the operational range of the μSTAMPS disc reservoir of 2.5 mm. The sensor's thin profile allows it to be integrated within the limited space available inside the thruster assembly. Bench-top tests and manufacturer data confirm the sensor's sensitivity and accuracy in detecting fluid levels across the entire measurement range. While attempts to optimize the propellant analogs conductivity yielded inconclusive results, it was determined that the capacitance sensor performs adequately regardless, provided the working fluid exhibits a minimum threshold of conductivity.

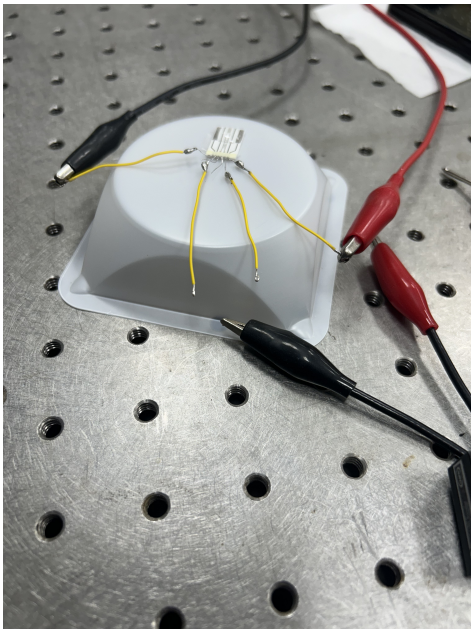


Figure 3.1: View of the test setup for the conductivity sensor.

3.2 Software Development, System Control, and Circuit Design

The control system for the propellant feed system was designed to function autonomously, integrating both software and hardware components to achieve reliable system behavior with minimal human intervention. A micro-controller platform was selected to serve as the core of the control system due to its adaptability, compactness, and ability to operate within the constraints typical of CubeSat environments. The software programmed onto the micro-controller is structured to interpret sensor feedback in real-time, determining appropriate system responses such as pump activation, reservoir replenishment, and system shut-off procedures. The embedded logic focuses on enabling the system to regulate propellant levels autonomously, while incorporating fault-tolerant features that ensure safe and robust operation during both ground testing and future flight scenarios.

Supporting this software, a circuit was developed to facilitate proper signal conditioning and power management. The circuit scales the sensor's output to levels compatible with the micro-controller and incorporates switching components to control the pump's power delivery. Design considerations include efficient power distribution, protection of sensitive electronics, and system modularity, all of which contribute to a design capable of supporting future scalability or adaptation to alternate thruster platforms. Power supplies external to the system are currently used for development purposes, but future iterations will integrate a consolidated power solution more appropriate for CubeSat deployment.

In conjunction with the hardware-software integration, a LabVIEW Virtual Instrument (VI) was created to visualize sensor data and control thresholds during system development. The VI serves as a diagnostic and analysis tool, providing a clear, real-time representation of system behavior, sensor outputs, and control logic performance. While the VI does not directly control hardware elements in this setup, its role is critical in offering insight into system dynamics and guiding design iterations. The intent behind the VI is to establish a comprehensive understanding of the system's function and interactions, providing a foundational perspective that informs hardware and software refinements moving forward.

The combined methodology behind the software development, system control, and circuit design prioritizes a balance of autonomy, simplicity, and flexibility. This approach is specifically tailored to meet the power, mass, and operational demands of space systems, supporting the ultimate goal of delivering a reliable and scalable propellant feed system for the μSTAMPS thruster.

3.3 Model Development, Fluid Routing, and Considerations

The methodology includes the design and refinement of a physical model to route fluid from the pump's tubing to the µSTAMPS disc reservoir. The model incorporates a funnel-like structure designed to direct the fluid flow past the capacitance sensor and into the reservoir, preventing fluid from pooling on the sensor surface. The fluid routing relies on geometric features such as ramps and guide channels that leverage surface tension and cohesive forces to control fluid movement. The system is designed to exploit capillary action within the reservoir while maintaining proper sensor exposure for accurate level readings.

The fluid routing model was iteratively refined based on experimental observations, with modifications made to funnel shapes, channel sizes, and reservoir interfaces to optimize flow behavior. Tests utilized water with adjusted conductivity via salt additive to simulate the ILs properties under terrestrial conditions, enabling practical evaluation of the model's effectiveness. While other factors may differ from those of the ILs, the main characteristic that affected these tests was the conductivity of the fluid. The salt water solution was mixed as a mass-based solution, where the mass of the salt used was measured, as seen by Fig. 3.2, to yield 25 mL of solution.



Figure 3.2: Image of the scale reading for the mass of salt used in the 25 mL solution.

In parallel with fluid routing considerations, design decisions prioritize system autonomy and efficiency. The circuit and control system were developed to minimize the need for manual operation and external intervention, reflecting CubeSat mission requirements. The use of the Arduino micro-controller provides a cost-effective and modular solution that enables system scalability and adaptability for future thruster configurations or mission profiles.

The power supply strategy is integrated into the design considerations, as power requirements play a key role in system simplicity and mass minimization. While external lab power supplies are used for current testing, future iterations will consolidate these into a unified, space-qualified power system. Emphasis is also placed on reducing component count and total system mass, supporting the overarching goal of producing a lightweight, efficient, and autonomous PFS suitable for CubeSat-class spacecraft.

Chapter 4

Results and Discussion

4.1 Subsystem Test Results

4.1.1 Sensor Validation

Following the prior shortcomings of the binary results from the conductivity sensor tests, a capacitance sensor was selected and required thorough validation. The primary operation of this sensor was dependent on its wiring configuration, as shown in Fig. 4.1. In accordance with manufacturer specifications, the sensor required +15 V, -15 V, and a ground connection to function correctly. The manufacturer's calibration documentation is presented in Table 4.1, where nominal VDC is expected output voltage, providing the error value. The sensor delivered an output voltage ranging from 0-10 V, subject to minor error, through a standard positive power and ground connection, also illustrated in Fig. 4.1. Although alternative power configurations could be implemented, such as a singular positive and ground supply, doing so would necessitate re-calibration of the sensor to ensure consistency with manufacturer-provided metrics. The power supply used for these tests provided the required +15 V and -15 V rails, is shown in Fig. 4.2. The +15 V and -15 V supply was verified by using a multimeter, in which it was found the true voltage varied from 14.6-15.2 V at peak points, for both positive and negative outputs. However, these values played a negligible role in the sensor's readings.

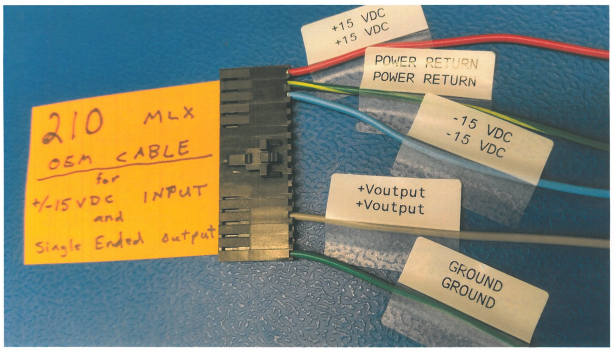


Figure 4.1: Image showing the required wiring setup for the sensor's operation.

Table 4.1: Calibration of Capacitance Sensor provided by the manufacturer.

Cal Points (mm)	Output (VDC)	Error	Nominal VDC
0.150	0.4528	-0.0472	0.5000
0.300	0.9991	-0.0009	1.0000
0.450	1.5371	0.0371	1.5000
0.600	2.0705	0.0705	2.0000
0.750	2.6005	0.1005	2.5000
0.900	3.1262	0.1262	3.0000
1.050	3.6495	0.1495	3.5000
1.200	4.1690	0.1690	4.0000
1.350	4.6846	0.1846	4.5000
1.500	5.1942	0.1942	5.0000
1.650	5.6981	0.1981	5.5000
1.800	6.1959	0.1959	6.0000
1.950	6.6842	0.1842	6.5000
2.100	7.1647	0.1647	7.0000
2.250	7.6352	0.1352	7.5000
2.400	8.0947	0.0947	8.0000
2.550	8.5429	0.0429	8.5000
2.700	8.9787	-0.0213	9.0000
2.850	9.4009	-0.0991	9.5000
3.000	9.8100	-0.1900	10.0000

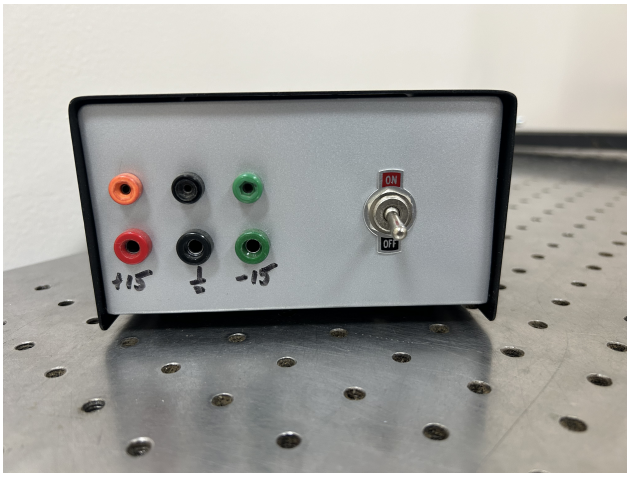


Figure 4.2: Image of the power supply used for the sensor, showing all power requirements.

Subsequently, preprocessing steps were implemented. The manufacturer's calibration data was curve-fitted and digitized and a best-fit equation was generated, seen in Fig. 4.3, to convert the sensor's voltage readings into corresponding fluid displacement measurements within the propellant reservoir. Furthermore, a refined calibration was conducted to enhance the linearity and precision of the sensor in the critical measurement range of 0.45 mm to 2.55 mm, the operative range for the propellant reservoir. This targeted calibration, or "super calibration,"is depicted in Fig. 4.4.

For hardware integration, a slot was inserted into the base of the model of the μSTAMPS model via SolidWorks remodeling, to house the sensor shown in Fig. 4.5. A LabVIEW VI was created for sensor testing and will be detailed in proceeding sections. Initial sensor validation was successful; tests confirm that a dry disc yielded no detectable fluid, while a disc saturated with a 35 % salt-water solution (process and specifics discussed previously in Sec. 3.3), approximating seawater conductivity for simulation of IL, triggered appropriate sensor readings. Although the numerical and visual data from this validation were lost, the operational performance of the sensor within the integrated environment was satisfactorily verified.

4.1.2 Fluid Flow Validation

With the sensor validated, fluid delivery required confirmation as well. The pump previously acquired for its potential use underwent testing to verify its flow rate and power consumption,

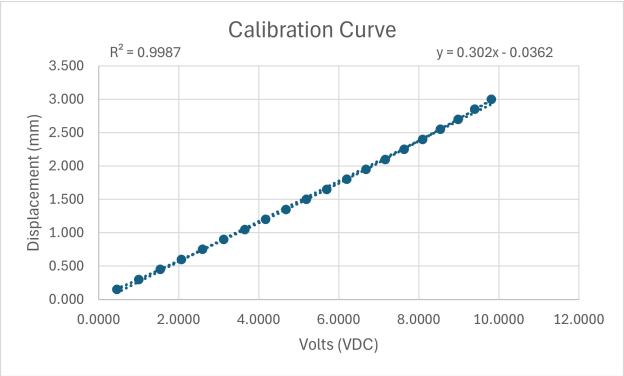


Figure 4.3: Graph showing the calibration data for 0 - 3 mm fitted to a linear function and the fit equation.

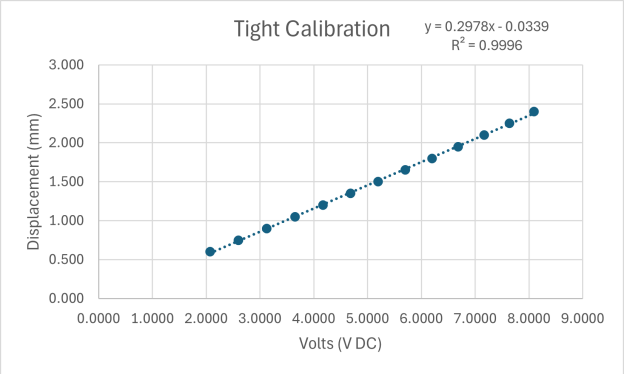


Figure 4.4: Graph showing the "super calibration" for the 0.6 - 2.4 mm range.

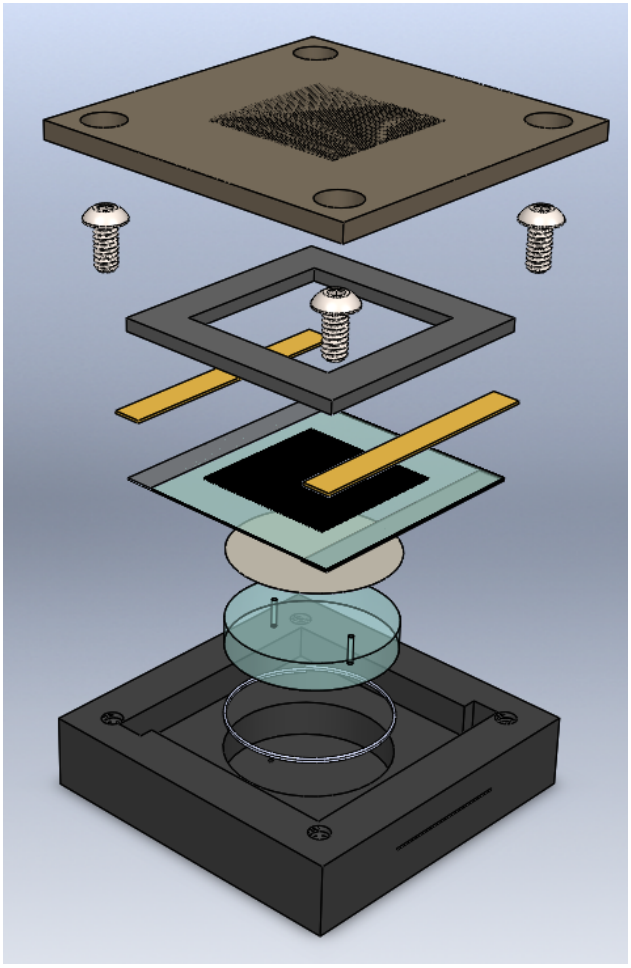


Figure 4.5: View of model assembly showing the slot at the lower right for the sensor.

as outlined in its specification sheet, seen in Table 4.2. Despite the pump being rated for 3 V and 0.4 mA operation, it was noted that applying higher voltages increased the flow rate; however, to preserve the pump's longevity (i.e., ensure the pump did not break), testing adhered to the recommended voltage. The confirmed flow rate under nominal conditions is shown in Table 4.3, and note that the flow rate specified pertains to a full tube flow rate.

A design challenge emerged from the spatial constraints within the reservoir. The sensor occupied a significant portion of the available room, seen in Fig. 4.6, limiting the area for fluid delivery into the 15 mm diameter porous disc. To address this, a funnel-shaped distribution component was designed to direct the fluid around the sensor and into the disc, seen in Figures 4.7 and 4.8. However, the small gaps within the funnel created issues with the cohesive and viscous nature of the liquids, leading to poor fluid transfer, an issue expected to be exacerbated by the reduced gravitational and pressure conditions of in-space applications, as well as these factors being enhanced with the use of IL. Consequently, a simplified side-entry model was developed to improve fluid entry into the disc, seen in Fig. 4.9. Multiple funnel designs were fabricated and tested, all exhibiting inadequate performance. Testing of the side-entry model with the pump and syringe setup is presented in Figures 4.10 and 4.11. Although life cycle validation was not achieved at this stage due to persistent flow restrictions, preliminary tests confirmed sufficient fluid delivery to the disc under ground conditions.

Table 4.2: Specifications and values of the pump given by the manufacturer.

Specification	**Value**
Dimensions	30 x 12 x 14mm
Flow Rate	0.45ml/min
Discharge Pressure	0 – 50kPa
Tube Size	OD 2.5mm, ID 1.5mm
Tube Length	60mm on inlet and outlet (approximate)
Tube Material	Silicone
Motor	DC Geared Motor
Voltage	3VDC
Power Consumption	0.12W
Weight	11g

Table 4.3: Peristaltic Pump tests at 3 V and 40 mA using a 60mL syringe.

Dry Mass (g)	Wet Mass (g)	Syringe Start (mL)	Total Time (s)	Flow Rate (g/s)	Flow Rate (mL/min)	Fluid in Pump (g)
2.9252	3.5017	20	132.81	0.005683162	0.340989748	0.1971
2.9249	3.489	19.2264	120.38	0.006757307	0.405438428	0.1936
2.925	3.5392	18.4687	120.35	0.007248908	0.439434498	0.2058
2.9251	3.5322	17.6487	120.37	0.00714824	0.428894384	0.1941
2.9278	4.803	16.8475	300.27	0.007049624	0.422977444	0.1915

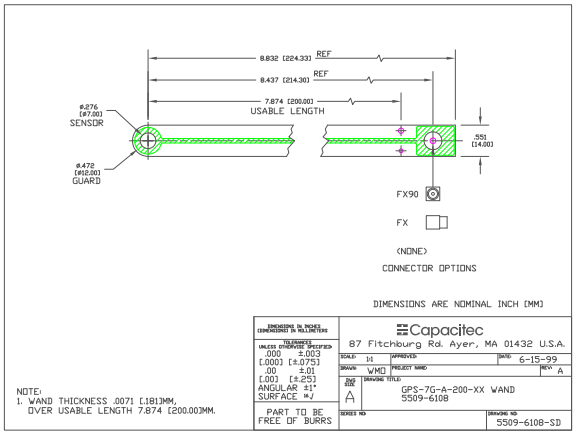


Figure 4.6: Diagram of the sensor's design per the manufacturer.

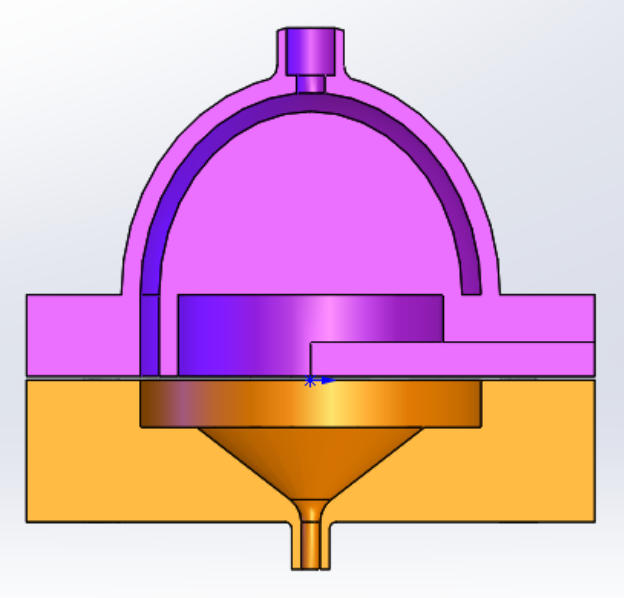


Figure 4.7: Interior view of the funnel model.

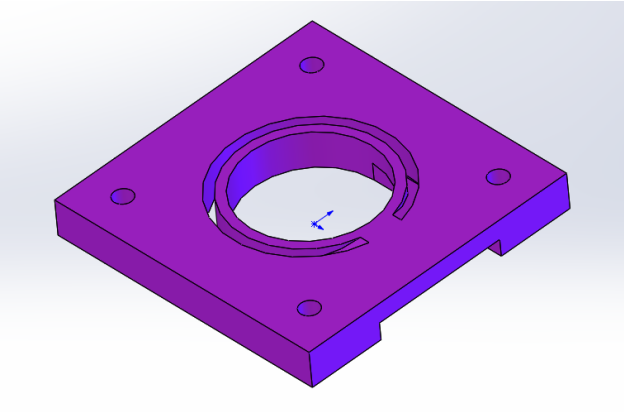


Figure 4.8: View showing the ramp in the funnel, moving liquid from over the sensor into the disc.

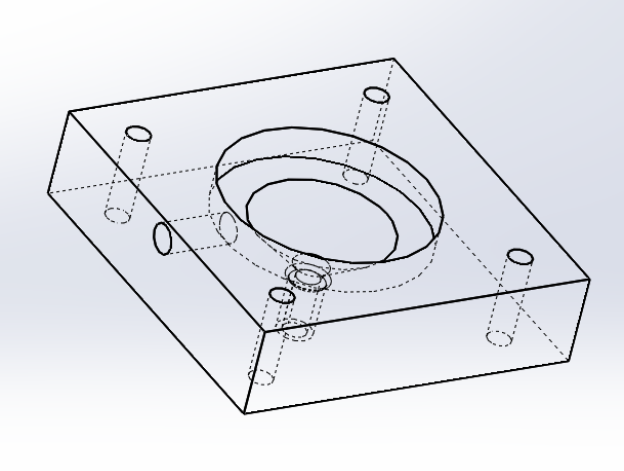


Figure 4.9: View of the side-entry model created, showing the through-hole for the tube placement.

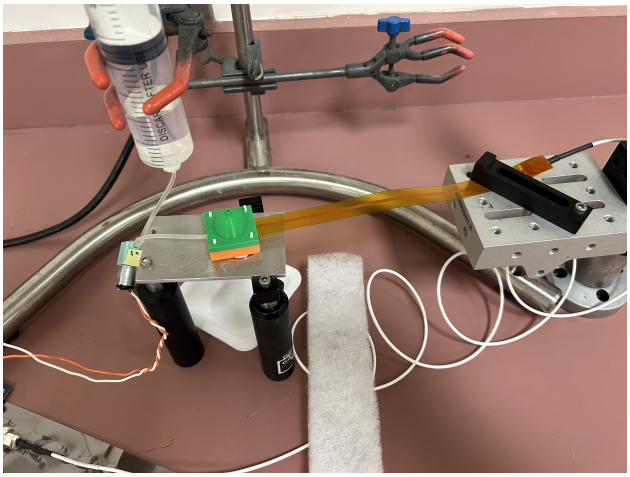


Figure 4.10: Depiction of the test setup with the side-entry model with syringe and pump.

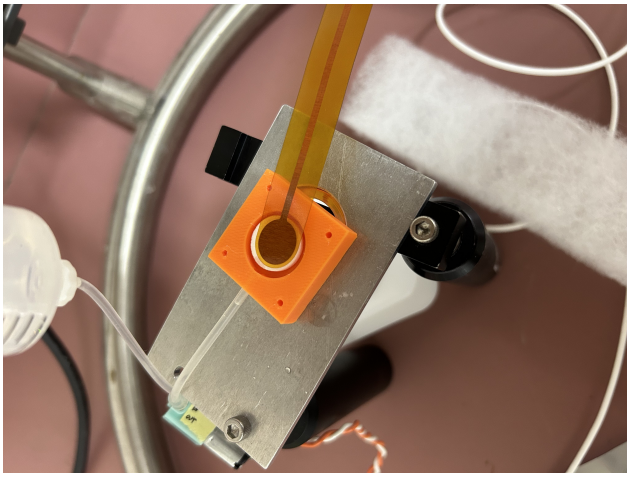


Figure 4.11: Depiction of the test setup without the sensor secured.

4.1.3 LabVIEW and Circuit Control

The sensor validation process required a LabVIEW VI capable of translating sensor voltage readings through the calibration curve and managing pump activation. The final LabVIEW interface used for these tests is presented in Fig. 4.12, with the corresponding wiring diagram shown in Figs. 4.13 and 4.14. Although initial efforts aimed to create a fully autonomous control loop within LabVIEW, limitations related to pump power delivery constrained this functionality. Nevertheless, the VI successfully interfaced with the sensor, processed voltage readings, and signaled the pump's activation to maintain the reservoir's propellant level (external triggering of the power supply was still required.)

To meet the objective of achieving autonomous system control without manual intervention, a micro-controller based circuit was subsequently developed. The circuit was designed and virtually tested using TinkerCad; its schematic is shown in Fig. 4.15, while its conceptual representation is provided in Fig. 4.16, and its physical system can be seen in Fig.4.17. The control algorithm implemented on the Arduino micro-controller is illustrated in Fig. 4.18 and 4.19, and its essential function was to process the sensor's voltage signal (0-10 V) using a voltage divider to scale it for the Arduino's 0-5 V operating range.

The program logic commanded the pump to activate when sensor voltage exceeded a 5 V threshold, indicating a reasonably low fluid level. Additionally, a safety feature was

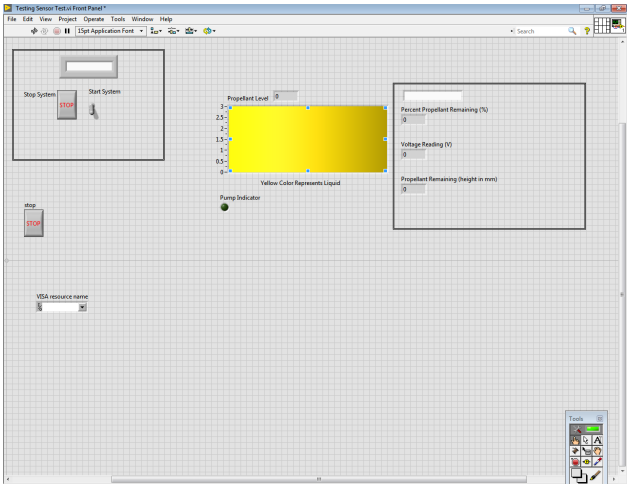


Figure 4.12: LabVIEW diagram showing the visual interface.

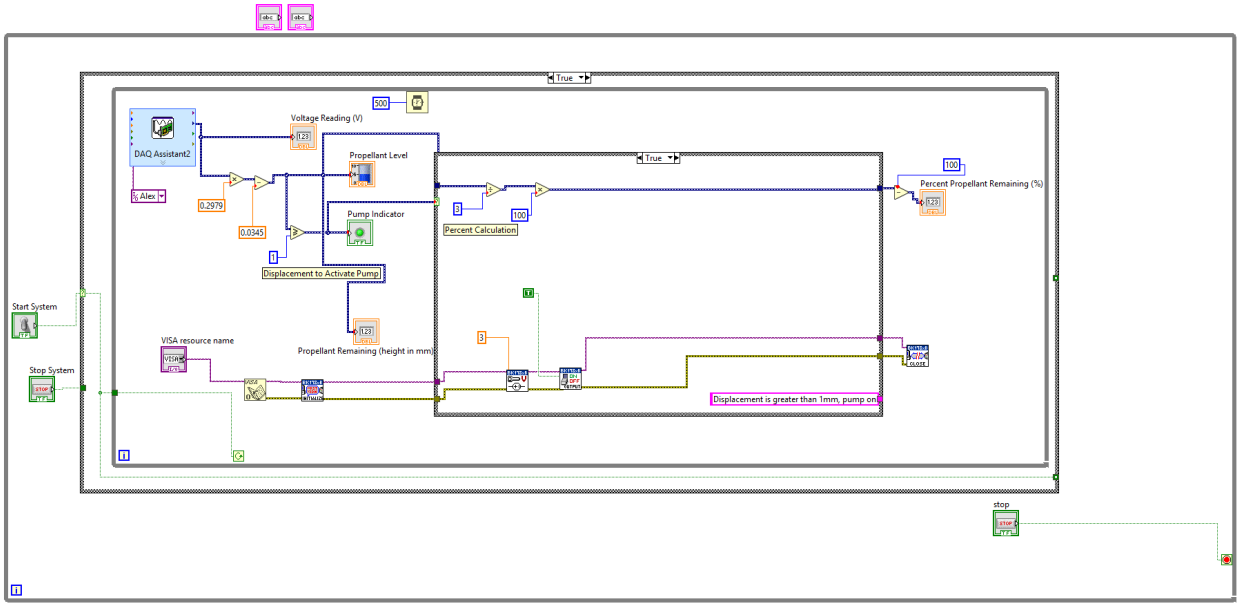


Figure 4.13: LabVIEW wiring diagram for the tested VI for the True case (run pump).

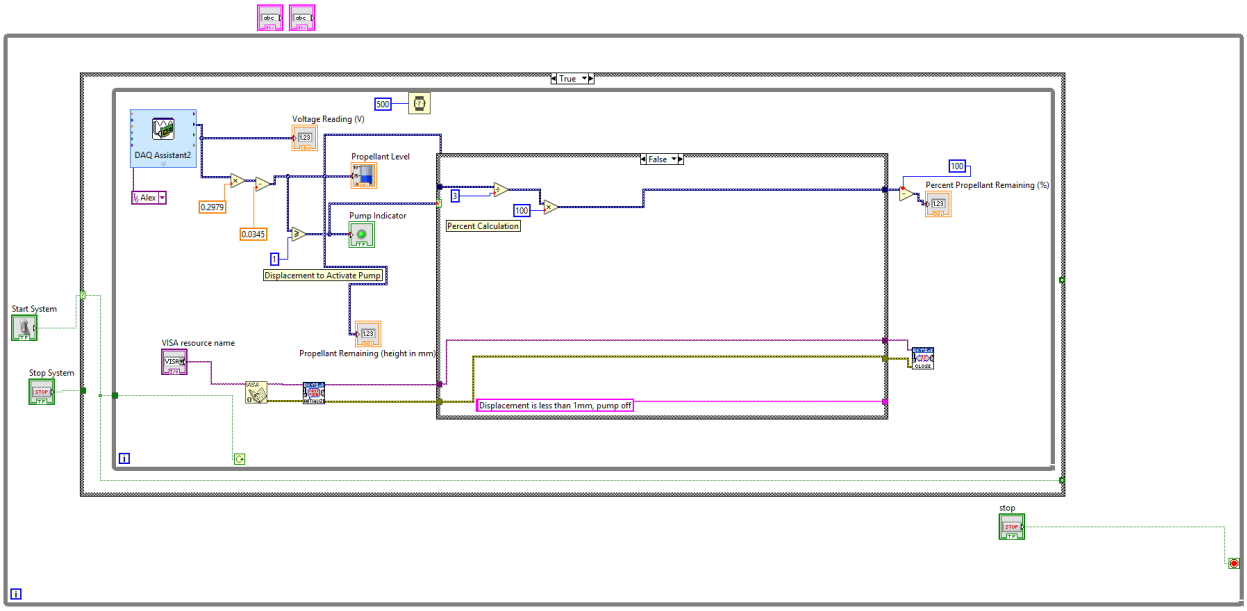


Figure 4.14: View of the false case (pump off) in the LabVIEW wiring diagram.

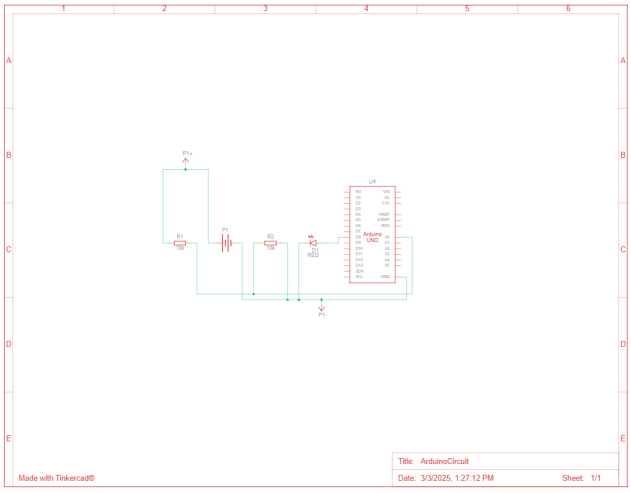


Figure 4.15: Developed circuit schematic from TinkerCad.

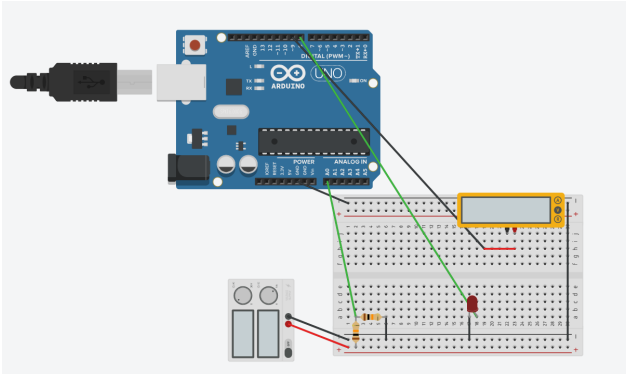


Figure 4.16: Depiction of the conceptual creation of the circuit in TinkerCad.

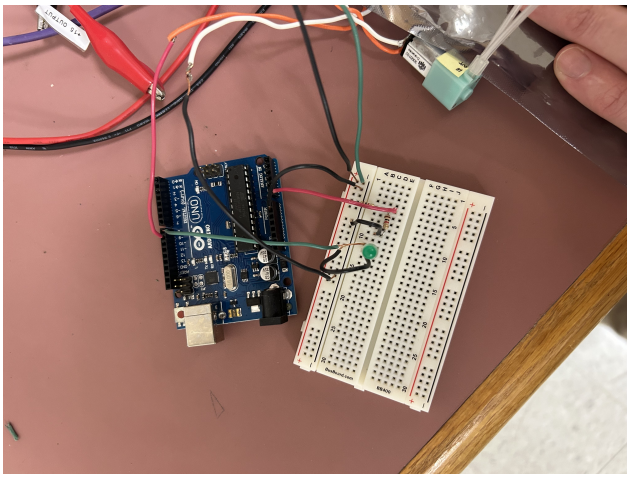


Figure 4.17: View of the physical circuit setup.

```
const int inputPin = A0; // Analog Pin for reading voltage from sensor
const int lightPin = 8; // Pin to control light (LED/lightbulb)
const int multimeterPin = 9; // Pin to control multimeter/Pump (3V output)
unsigned long timerStart = 0; // Variable to store the start time when voltage reaches 10V
bool lightOn = false; // Flag to check if light is already on.
float previousVoltage = -1.0; // Variable to store previous value
bool systemShutdown = false; // Flag to check if system shutdown message was already used.


void setup() {
    pinMode(lightPin,OUTPUT); // Set lightPin as output for LED
    pinMode(multimeterPin,OUTPUT); // Set multimeterPin as output for 3V supply
    Serial.begin(9600); // for debugging
}

void loop() {
    // Check if light is on, stop the system if so
    if (lightOn) {
        if (!systemShutdown){
            // Print shutdown message once
            Serial.println("System shutdown");
            systemShutdown = true; // Update and print once
        }
        analogWrite(multimeterPin,0); // make sure power is cut off
        digitalWrite(lightPin, HIGH); // Keep LED on
        Serial.println("System shutdown.");
        return; // Exit this loop
    }

    // read the input voltage from the power supply
    int sensorValue = analogRead(inputPin);

    // Convert the ADC Value to Voltage
    float voltage = sensorValue * (10.0/1023); // Convert ADC value to Voltage (0-5V) ** This has issues and should  be revisited**
```

Figure 4.18: Part 1 of the Arduino code used, should be split into subplots to include them both.

```
35
36 //Only print if voltage changes
37 if (voltage != previousVoltage) {
38     previousVoltage = voltage; //Update previous voltage value
39     Serial.print("Input Voltage: ");
40     Serial.println(voltage);
41 }
42
43     // if voltage is 5v or greater, supply 3V to the multimeter (via PWM)
44     if (voltage >=5.0){
45         if (!systemShutdown){
46             analogWrite(multimeterPin,153); // Output PWM value, should be 3V
47             Serial.println("Supplying ~3V to the multimeter");
48             //If 10V is detected, start timer for system shut-off
49             if (voltage >=10){
50                 if (timerStart == 0){
51                     timerStart = millis();
52                     Serial.println("Timer started, 10V detected");
53             }
54                 if (millis() - timerStart >= 60000) {
55                     if (!lightOn) {
56                         analogWrite(multimeterPin,0); // Turns off multimeter
57                         digitalWrite(lightPin, HIGH); // turn on LED
58                         lightOn = true; //Note light is on
59                         Serial.println("LED turned on, system shut off");
60                     }
61                 }
62             }
63         }
64     } else {
65         analogWrite(multimeterPin,0); // Output 0V to turn off supply
66         Serial.println("No power to multimeter");
67     }
68     delay (1000); // Delay for stability
69
70     }
71
72
```

Figure 4.19: Continuation of the Arduino code used, from Fig. 4.18.

implemented where, if the sensor reading reached 10 V and remained constant for a set duration, the system would power down and provide a signal via an LED indicator (as well as a message in the serial monitor), to preserve power for the CubeSat application. As mentioned, serial monitoring was employed during testing for verification purposes, though it is not intended (needed) for the final system.

It's important to note that minor discrepancies were observed between sensor readings and serial monitor outputs, likely due to internal resistance within the circuit. This internal resistance changed the output displayed by the Arduino from the 0-10 V range to more of a 1.5-9.1 V range (on average). These variations were negligible in the performance for this variation of the system, but did necessitate slight adjustments to programmed voltage thresholds.

4.2 Integrated System Performance

The final integrated system, consisting of the capacitance sensor, fluid routing models, pump, and control circuitry, was assembled and evaluated under laboratory conditions. The testbed included the μSTAMPS model positioned on a raised platform with an outlet gap, a syringe simulating the propellant tank, the pump, and all necessary control electronics. Multiple views of the full system setup and test environment are provided in Figures 4.20 and 4.21.

The sensor was mounted within the model reservoir, inserted into a designed slot that secured it above the porous disc shown in Fig. 4.22 (will be placed below the disc in final system integration with the μSTAMPS thruster). This positioning allowed the sensor to directly monitor fluid levels within the disc securely, interfacing seamlessly with the integrated circuit (IC) board shown in Fig. 4.23. The sensor's calibrated output range, as detailed in the super calibration curve (Fig. 4.4), provided a precise voltage-to-fluid height conversion critical to having an understanding of the system.

The fluid routing models presented operational constraints during testing. The funnel design, developed to direct fluid from the pump outlet around the sensor and into the disc (Fig. 4.22), exhibited incomplete fluid path connection (wetting) and flow blockages due to the limited gap clearance and the fluid's cohesive properties, seen in Fig. 4.24. This inhibited any saturation of the disc. Furthermore, the lab conditions included higher pressure and a presence of gravity affecting this fluid flow that would not be present in space-like conditions (vacuum and microgravity). This spatial conflict between sensor placement and fluid routing geometry necessitated the development of the alternate, side-entry model, depicted in Fig. 4.9, which improved flow conditions but did not fully resolve exit flow restrictions during the tests seen in Figures 4.25 and 4.26. The side-entry model on the other hand, proved successful with the internal reservoir filling up without leakage, seen in Fig. 4.25; however, there was still a persisting issue regarding fluid exiting the model.

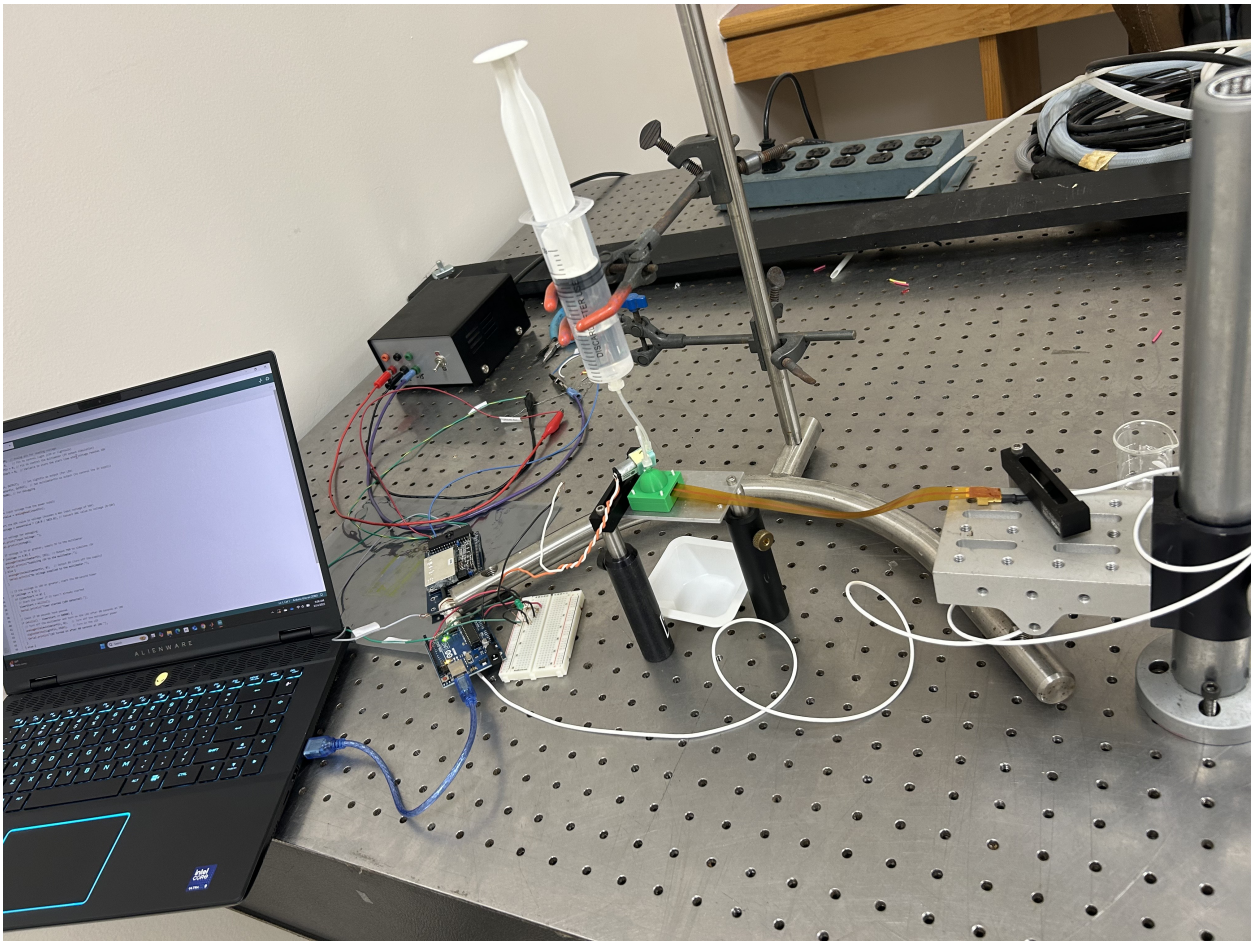


Figure 4.20: View of the full setup used for testing.

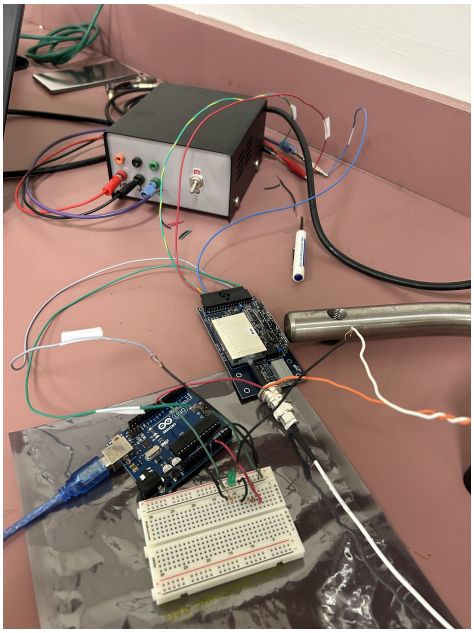


Figure 4.21: View of the electronics setup/wiring for testing.

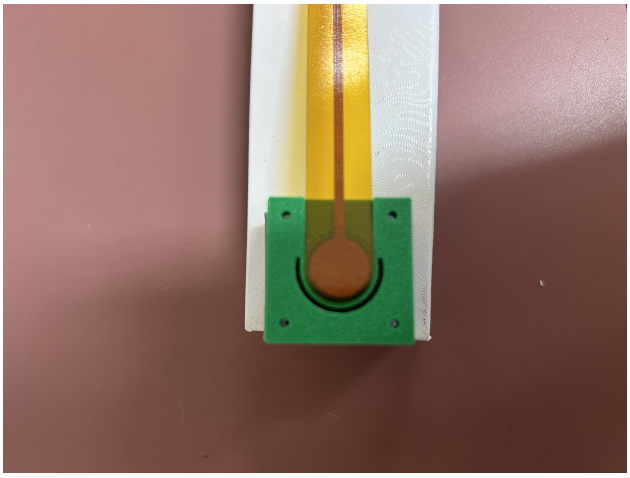


Figure 4.22: Image of the sensor fitted and secured into its slot.

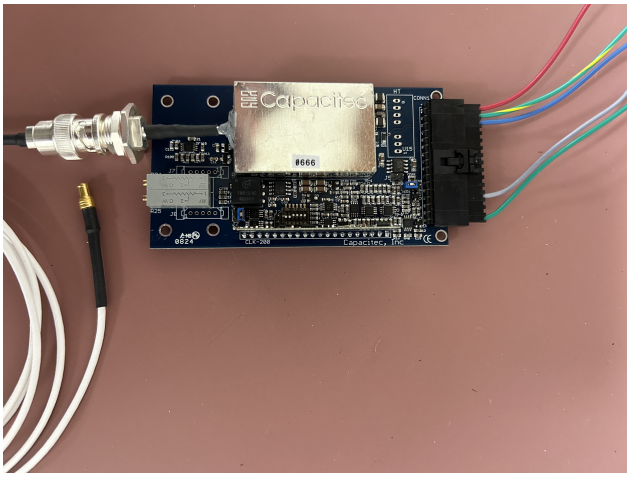


Figure 4.23: View of the sensors Integrated Circuit board with wiring.

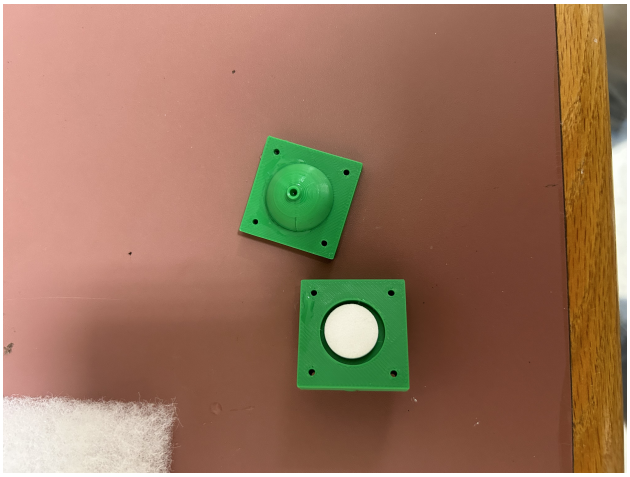


Figure 4.24: Image of a dry disc and inside, with a wet top post fluid-routing-test.

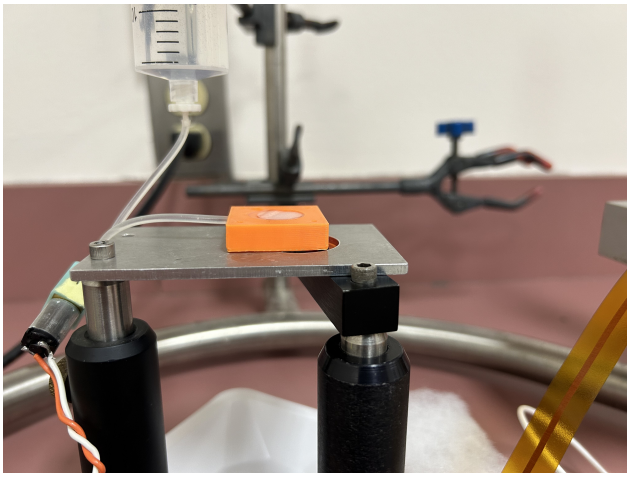


Figure 4.25: View of the full internal reservoir post-test.

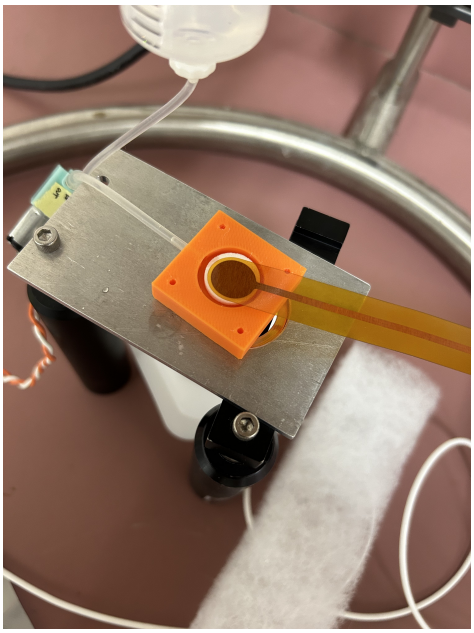


Figure 4.26: View of the full internal reservoir post test with the sensor present at the top.

The initial testing via the LabVIEW VI demonstrated effective sensor interfacing and pump activation logic based on voltage thresholds derived from the sensor calibration curve. The LabVIEW front panel and wiring diagram used during these tests were shown in Figs. 4.12 and 4.13 respectively. Despite this success, limitations with powering the pump directly from LabVIEW necessitated the development of an external circuit for full automation. The result of that was an Arduino-based control circuit, seen in Fig. 4.23, which incorporated a voltage divider to scale the sensor's 0-10 V output to a 0-5 V range compatible with the Arduino's analog input. Control logic was implemented to activate the pump when the sensor voltage exceeded 5 V, representing an under-filled reservoir. A safety/shutoff feature was also embedded, whereby the circuit triggered a system shutdown and indicator signal when the sensor voltage approached the maximum 10 V, representing a "dry"reservoir condition with no propellant left in the tank. During testing, this circuit provided autonomous control over the pump based on real-time sensor feedback, validating its effectiveness of the control sequence, including pump activation/deactivation and triggering of the LED indicator when appropriate. However, it was noted that the sensor voltage readings displayed on the serial monitor deviated slightly from direct measurements from sensor itself/LabVIEW, likely due to internal resistance within the voltage divider/circuit network. This discrepancy was

consistently observed across multiple trials but was mitigated via code-level adjustments, offsetting the control thresholds to match the system behavior. Although this offset was manageable, it introduced a layer of complexity into system calibration that will need to be addressed for future iterations.

The integrated system achieved autonomous reservoir filling, with the pump activating as intended based on sensor voltage readings and ceasing operation upon reaching the timer threshold. Nonetheless, persistent issues with fluid outflow from the model's base prevented a complete fluid life-cycle (fill to drain and repeat). While this limitation did not affect the validation of the PFS's ability to autonomously control reservoir fluid levels, it did restrict the scope of full-system testing under ground conditions.

4.3 Successes and Limitations

The integrated system testing yielded several critical successes in the development and validation of the PFS for the μSTAMPS platform. Foremost, the capacitance sensor was successfully validated both in isolation and within the full system, demonstrating accurate and repeatable fluid level detection within the calibrated range. The calibration curve, seen in Fig. 4.3, and sensor integration into the model reservoir provided consistent and interpretable voltage readings, supporting autonomous decision-making for reservoir refilling.

The pump performed within its specified parameters, providing fluid transport at a validated flow rate once tubing was primed. When integrated with the control system, the pump effectively responded to sensor-driven commands to fill the reservoir without human interface. Additionally, the Arduino-based control circuit successfully processed scaled sensor signals and executed control logic for activating and deactivating the pump. The system operated independently of human input once power was supplied, validating the concept of autonomous reservoir maintenance suitable for small satellite platforms.

The use of the LabVIEW VI further contributed to system development by enabling sensor calibration, threshold testing, and initial pump signaling, though its role was ultimately limited due to constraints in control of the pump's power supply.

Despite these successes, several limitations were identified during testing. The fluid routing models exhibited significant challenges stemming from spatial interaction between the sensor and the funnel geometry. The small gaps between the sensor and funnel walls limited fluid ingress into the disc, resulting in flow stagnation and incomplete disc saturation. Although the side-entry model improved this behavior, it did not fully mitigate the issue of restricted outflow from the disc to the catch basin. Furthermore, the circuit exhibited minor but consistent voltage reading discrepancies between the sensor output and Arduino serial monitor data, attributed to internal resistance within the voltage divider network. While these offsets were corrected through code modification, this represents an additional calibration step and potential variability source that will need to be addressed in future circuit iterations. Additionally, timing considerations related to the pump's tubing fill and empty cycles emerged as an important factor influencing system control logic. The control code requires tuning to accommodate delays associated with priming and draining the tubing, a parameter that will vary depending on final system layout and component selection. Lastly, full cycle validation, encompassing complete reservoir fill, drain, and refill, was not achieved due to persistent flow restrictions within the model during testing. While this could have been changed and adjusted, it does not compromise validation of the PFS's autonomous reservoir filling capability; simply limiting the life-cycle tests which are unnecessary at the current stage of the system.

Chapter 5

Conclusion and Future Work

5.1 Conclusions

This project successfully demonstrates the preliminary development and validation of a scalable and autonomous PFS designed specifically for the μSTAMPS thruster. The integration of a capacitance-based sensor proved highly effective, providing accurate and repeatable measurements of fluid displacement, which is essential for CubeSat propulsion. The comprehensive calibration efforts, including the generation of both calibration curves, ensured more precise sensor functionality within the integrated reservoir environment.

Significant achievements include the successful integration of autonomous control circuit based on Arduino technology, demonstrating reliable operation in sensor signal interpretation and responsive pump control. The designed circuitry effectively managed voltage scaling, sensor interfacing, and power distribution, ensuring autonomous, safe, and responsive operations without the need for external intervention once activated. This represents an essential step toward achieving fully autonomous micro-propulsion systems for CubeSats, significantly enhancing their potential for complex and extended-duration missions.

Moreover, iterative development of fluid routing models highlighted crucial considerations in managing fluid dynamics within micro-scale systems. Although initial funnel-based designs experience challenges related to fluid ingress and egress due to cohesion effects and spatial constraints, subsequent iterations, including the side-entry model, improved fluid management, successfully demonstrating effective reservoir filling under laboratory

conditions. These iterative improvements emphasized the importance of careful geometric considerations in microfluidic system designs, particularly relevant in space-based applications where gravitational assistance is absent.

However, the development phase also revealed crucial limitations. Persistent challenges with complete fluid flow through the reservoir highlight the complexities involved in achieving efficient fluid management in constrained geometries, especially under microgravity conditions expected during CubeSat missions. Furthermore, minor discrepancies in sensor voltage readings observed within the circuit setup indicated the need for a more robust internal electrical design, particularly addressing the voltage division and resistance characteristics. Although manageable through software adjustments, these issues underscore potential areas for improvement in future iterations.

In conclusion, the developed PFS demonstrated significant potential, successfully meeting the initial project objectives of autonomous propellant management and scalability. The groundwork laid through this project establishes a solid foundation for future advancements in micro-propulsion technology tailored though explicitly for CubeSats. Continued refinement of fluid routing geometry, electrical circuit robustness, and comprehensive life-cycle testing will further enhance system performance and reliability, positioning the μSTAMPS thruster system for increasingly demanding space missions.

5.2 Future Work

Future work should initially focus on refining and optimizing the circuitry to better suit the constraints and operational demands inherent to CubeSat missions. Given the current capabilities and functionalities demonstrated by the existing circuit, transitioning to a micro-Arduino platform is advisable. This transition not only aligns with stringent size and mass constraints typical of CubeSat deployments, but also enhances system integration and operational reliability. Once miniaturization is achieved, permanent soldering of the circuit components is recommended to enhance durability and reduce susceptibility to mechanical and electrical failures.

Subsequently, developing a dedicated, robust housing for the integrated system, including circuitry, sensor, and pump, is essential. This housing should be meticulously designed to accommodate the sensor's dimensional and environmental requirements, potentially necessitating a custom-ordered or modified sensor to ensure compatibility and optimal functionality within the redesigned system architecture.

An integral component of future enhancements involves designing or selecting an appropriate propellant tank. A practical and effective solution could be a modified syringe-based tank, carefully engineered according the the pressure requirements documented by the pump specification sheet. Incorporating a detachable filling stem during manufacturing or propellant loading stages would significantly simplify operations, minimize cost, and facilitate seamless integration into CubeSat platforms.

Should these advancements encounter implementation challenges or operational inefficiencies, an alternative approach would be to revisit the control and sensing methodology fundamentally. This alternative would abandon the capacitance-based sensor system, favoring a more traditional, reliability oriented approach reminiscent of Apollo-era techniques. Such a method would utilize a mechanical or digital counting system (bookkeeping method) to track fluid usage intervals. This approach would enable straightforward fluid delivery into the disc reservoir but would require accepting inherent operational limitations and reduce flexibility compared to the sensor-based automation. Ultimately, these future efforts will guide the μSTAMPS PFS development toward achieving enhanced robustness, efficiency, and reliability, ensuring its readiness for complex and demanding CubeSat missions in the near future.

Bibliography

[1] Hank Heidt, Jordi Puig-Suari, Augustus S. Moore, Shinichi Nakasuka, and Robert J. Twiggs. Cubesat: A new generation of picosatellite for education and industry low-cost space experimentation. In Technical Session V: Lessons Learned - In Successes and Failure. *Proceedings of the 14th Annual AIAA/USU Conference on Small Satellites*, 2000, paper SSC00-V-5. 1, 3

[2] Cal Poly SLO The CubeSat Program. Cubesat design specification rev. 14.1. http://www.cubesat.org, 2014. Accessed: [2025-06-04]. ix, 1, 2, 3, 4

[3] Akshay Reddy Tummala and Atri Dutta. An overview of cube-satellite propulsion technologies and trends. *Aerospace*, 4(4):58, 2017. http://dx.doi.org/10.3390/aerospace4040058. viii, ix, 1, 3, 4, 6, 16, 17, 18, 19

[4] NanoSats Database. Nanosats database. https://www.nanosats.eu/, 2025. Accessed: 2025-06-04. ix, 5

[5] Trevor Moeller, Lino Costa, Alexander Terekhov, and Brian Canfield. Concept design of μSTAMPS thruster volume 1, 2022. Unpublished. ix, 6, 7, 8, 9, 10, 11, 12, 24

[6] Trevor Moeller, Lino Costa, Alexander Terekhov, Brian Canfield, Caitlin Bunce, Joshua Howell, Adam Huller, and Tyler Sundstrom. Station-keeping, collision avoidance, and rapid deorbit of nanosatellites: A comparison of micro-propulsion systems. Technical report, University of Tennessee Space Institute, December 2022. ix, 6, 8, 10, 24

[7] Trevor Moeller, Lino Costa, Justin Jones, Alexander Terekhov, and Brian Canfield. Demonstration of dual mode ionic liquid propulsion: NASA phase 1 STTR final report. Technical report, University of Tennessee Space Institute, September 2020. Final report to Streamline Automation, LLC for NASA Phase 1 STTR award. 8, 10

[8] Brian K. Canfield, Lino Costa, D. Rajput, Alexander Terekhov, K. Lansford, W.H. Hofmeister, and L.M. Davis. Machining of micrometer-scale high aspect ratio features with single femtosecond laser pulses. *Journal of Laser Applications*, 32(3):032021, 2020. https://doi.org/10.2351/7.0000147. 8, 10

[9] Eric E. D'Ambro. Design of a thrust stand using impingement force on a weigh cell from an electric micro-propulsion thruster. Master's Project, University of Tennessee Space Institute, May 2023. 8, 10

[10] Justin M. Jones, Trevor M. Moeller, Lino Costa, Brian K. Canfield, and Alexander Terekhov. Numerical investigation of the effects of geometry and materials on the onset voltage of electrospray emitters. *Journal of Electrostatics*, 108:103487, 2020. https://doi.org/10.1016/j.elstat.2020.103487. 8

[11] a.i. Solutions. FreeFlyer Software. https://ai-solutions.com/, Jul 2023. 8

[12] Khary I. Parker and David C. Folta. Chatper 15: Propulsion system. In *CubeSat Handbook: From Mission to Operations*, 2021. Available at https://ntrs.nasa.gov/citations/20205003834. ix, 15, 16

[13] Kurt A. Polzin. Iodine hall thruster propellant feed system for a cubesat. In *50th AIAA/ASME/SAE/ASEE Joint Propulsion Conference*, Cleveland, OH, July 2014, paper AIAA 2014-3915. https://doi.org/10.2514/6.2014-3915. ix, 17, 18

[14] Ivan Martinez I Cano and Kenneth D. Mease. Electrospray propulsion performance for cubesat missions. In *AIAA SciTech Forum*, National Harbor, MD, January 2023. https://doi.org/10.2514/6.2023-2645. 17

[15] Louis E. Perna, Fernando Mier Hicks, Chase S. Coffman, Hanqing Li, and Paulo C. Lozano. Progress toward demonstration of remote, autonomous attitude control of a cubesat using ion electrospray propulsion systems. In *48th AIAA/ASME/SAE/ASEE Joint Propulsion Conference & Exhibit*, Atlanta, Georgia, July 2012. https://doi.org/10.2514/6.2012-4289. 17

[16] Amelia Greig, Antonio B. Robali, Catherine M. Carrillo, and Alberto Meza. Design and testing of a cubesat rail integrated electrospray thruster. In *Electrospray Thrusters I: AIAA Propulsion and Energy Forum*, Virtual Event, August 2021, paper AIAA 2021-3421. https://doi.org/10.2514/6.2021-3421. 18

[17] G. Lenguito, J. Frenandez de la Mora, and A. Gomez. Multiplexed electrospray for space propulsion applications. In *48th AIAA/ASME/SAE/ASEE Joint Propulsion Conference & Exhibit*, Nashville, TN, July 2010, paper AIAA 2010-6521. https://doi.org/10.2514/6.2010-6521. 18

[18] Jared L. Pilcher. Comparison of decision analysis methods for a cubesat propulsion system. Master's thesis, Air Force Institute of Technology, Dayton, OH, March 2021. 18

[19] Suood Alnaqbi, Djamal Darfilal, and Sean Shan Min Swei. Propulsion technologies for cubesats: Review. *Aerospace*, 11(7):502, 2024. https://doi.org/10.3390/aerospace11070502. 18

[20] Paul R. Chiarot, Pierre Sullivan, and Ridha Ben Mrad. An overview of electrospray applications in MEMS and microfluidic systems. *Journal of Microelectromechanical Systems*, 20(6):1241–1249, December 201. http://dx.doi.org/10.1109/JMEMS.2011.2168810. 18

[21] David Krejci, Fernando Mier-Hicks, Corey Fucetola, Paulo Lozano, Andrea Hsu, and Francois Martel. Design and characterization of a scalable ion electrospray propulsion system. In *Joint Conference of 30th International Symposium on Space Technology and Science. 34th International Electric Propulsion Conference, and 6th Nano-satellite Symposium*, July 2015, Paper IEPC-2015-149. 18

[22] D. O'Reilly, G. Herdrich, and D. F. Kavanagh. Electric propulsion methods for small satellites: A review. *Aerospace*, 8(1):22, 2021. https://doi.org/10.3390/aerospace8010022. 19

[23] Ellen Bausback. NASA tests new spacecraft propellant gauge on lunar lander. https://www.nasa.gov/centers-and-facilities/glenn/nasa-tests-new-spacecraft-propellant-gauge-on-lunar-lander, Feb. 2024. Accessed: 2025-06-04. 19, 21

[24] Jed Storey, Brandon Marshall, Mike Elmore, and Scott Clark. Preliminary results from propellant mass guaging in microgravity with electrical capacitance tomography. https://ntrs.nasa.gov/citations/20220010165, Sept. 2022. Accessed: 2025-06-04. 19

[25] Christian Bihr, Flavio Murolo, Milan Klinc, Issam Maurice Achkar, and Bernard Robert. Propellant gauging experience with meteosat second generation s/c fleet. *2018 SpaceOps Conference*, May 2018. https://doi.org/10.2514/6.2018-2319. 19, 20

[26] atout. SMARTTS: Smart tanks for space. https://www.smarttanksforspace.co.uk/, 2024. Accessed: 2025-06-04. 20

[27] Atlas Scientific. How do conductivity meters work? https://atlas-scientific.com/blog/how-do-conductivity-meters-work/?srsltid=AfmBOor9UD2hmxQbLRESjg1frT5-wWwT-4gUZEmTTVBaTL_RwPI4JJ5u, Nov 2022. Accessed: 2025-06-04. 20

[28] NASA. Streamlined liquid level sensing using fiber optics. Technology brief. https://technology.nasa.gov/patent/DRC-TOPS-16, 2025. Accessed: 2025-06-04. 20

[29] Andres Aparicio and Boris Yendler. Thermal propellant gauging at EOL, Telstar 11 implementation. *In EOL-1: End-Of-Life Operations and Space Debris I, SpaceOps 2008 Conference*, May 2008, paper AIAA 2008-3375. https://doi.org/10.2514/6.2008-3375. 21

[30] Paulo Cesar Lozano-Tovar. *Studies on the ion-droplet mixed regime in colloid thrusters*. PhD thesis, Massachusetts Institute of Technology, 2003. 22

[31] Chase S. Coffman, Daniel G. Courtney, Fernando M. Hicks, Sara Jamil, Hanqing Li, and Paulo Lozano. Progress toward a variable specific impulse electrospray propulsion system. *In 47th AIAA/ASME/SAE/ASEE Joint Propulsion Conference & Exhibit. August 2011, paper AIAA 2011-5591*, https://doi.org/10.2514/6.2011-5591. 22, 23

[32] Manel Caballero-Pérez, Marc Galobardes, and Manuel Gamero-Castaño. High specific impulse electrospray propulsion with small capillary emitters, 04 2025. http://dx.doi.org/10.48550/arXiv.2504.00474. 22, 23

[33] John K Ziemer, Colleen Marrese-Reading, Steven Arestie, Nathaniel Demmons, Richard Wirz, Adam Collins, and Manuel Gamero. Electric Propulsion Microthrusters for Spacecraft Precision Pointing and Attitude Control, lecture, nesc academy (NASA engineering and safety center), 2020. Access from https://nescacademy.nasa.gov/video/c45d62*efe9d43a9bb2166781ba0e211d. 22

[34] Albert Cisquella-Serra, Marc Galobardes-Esteban, and Manuel Gamero-Castaño. Scalable microfabrication of multi-emitter arrays in silicon for a compact microfluidic electrospray propulsion system. *ACS Applied Materials & Interfaces*, 14, 09 2022. http://dx.doi.org/10.1021/acsami.2c12716. 22, 24

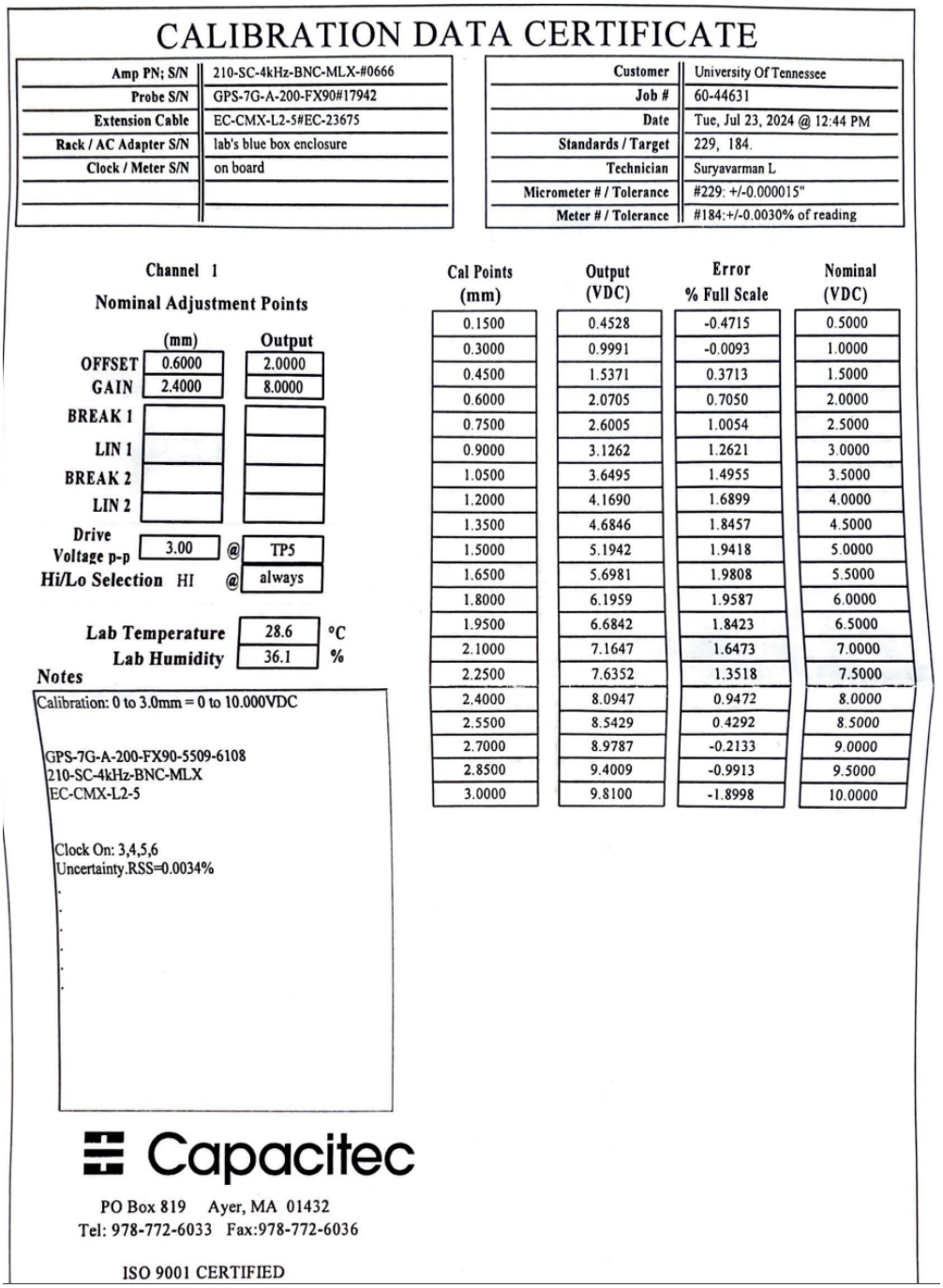
[35] Marc Galobardes, Albert Cisquella Serra, Marco Magnani, and Manuel Gamero-Castaño. Electrospray propulsion propellant feed subsystem development. In S1-1: Sub-Systems, 38th International Electric Propulsion Conference IEPC, June 2024, paper IEPC-2024-823. 22, 23, 24

[36] Marsil A. C. Silva, Daduí C. Guerrieri, Angelo Cervone, and Eberhard Gill. A review of MEMS micropropulsion technologies for CubeSats and PocketQubes. *Acta Astronautica*, 143:234–243, 2018. https://doi.org/10.1016/j.actaastro.2017.11.049. 23, 24

[37] T. M. Sundstrom. Conceptual propellant feed system for electrospray thrusters. Master's thesis, University of Tennessee, Knoxville, 2024. 24

Appendices

A Full Calibration Sheet



CALIBRATION DATA CERTIFICATE

Amp PN; S/N	210-SC-4kHz-BNC-MLX-#0666
Probe S/N	GPS-7G-A-200-FX90#17942
Extension Cable	EC-CMX-L2-5#EC-23675
Rack / AC Adapter S/N	lab's blue box enclosure
Clock / Meter S/N	on board

Customer	University Of Tennessee
Job #	60-44631
Date	Tue, Jul 23, 2024 @ 12:44 PM
Standards / Target	229, 184.
Technician	Suryavarman L
Micrometer # / Tolerance	#229: +/-0.000015"
Meter # / Tolerance	#184:+/-0.0030% of reading

Channel 1

Nominal Adjustment Points

	(mm)	Output
OFFSET	0.6000	2.0000
GAIN	2.4000	8.0000
BREAK 1		
LIN 1		
BREAK 2		
LIN 2		

Drive Voltage p-p: 3.00 @ TP5

Hi/Lo Selection HI @ always

Lab Temperature: 28.6 °C

Lab Humidity: 36.1 %

Notes

Calibration: 0 to 3.0mm = 0 to 10.000VDC

GPS-7G-A-200-FX90-5509-6108
210-SC-4kHz-BNC-MLX
EC-CMX-L2-5

Clock On: 3,4,5,6
Uncertainty.RSS=0.0034%

Cal Points (mm)	Output (VDC)	Error % Full Scale	Nominal (VDC)
0.1500	0.4528	-0.4715	0.5000
0.3000	0.9991	-0.0093	1.0000
0.4500	1.5371	0.3713	1.5000
0.6000	2.0705	0.7050	2.0000
0.7500	2.6005	1.0054	2.5000
0.9000	3.1262	1.2621	3.0000
1.0500	3.6495	1.4955	3.5000
1.2000	4.1690	1.6899	4.0000
1.3500	4.6846	1.8457	4.5000
1.5000	5.1942	1.9418	5.0000
1.6500	5.6981	1.9808	5.5000
1.8000	6.1959	1.9587	6.0000
1.9500	6.6842	1.8423	6.5000
2.1000	7.1647	1.6473	7.0000
2.2500	7.6352	1.3518	7.5000
2.4000	8.0947	0.9472	8.0000
2.5500	8.5429	0.4292	8.5000
2.7000	8.9787	-0.2133	9.0000
2.8500	9.4009	-0.9913	9.5000
3.0000	9.8100	-1.8998	10.0000

Capacitec

PO Box 819 Ayer, MA 01432
Tel: 978-772-6033 Fax:978-772-6036

ISO 9001 CERTIFIED

Figure A.1: Calibration sheet provided by the manufacturer

B Pump Specification Sheet

Specification	Value
Dimensions	30 x 12 x 14mm
Flow Rate	0.45ml/min
Discharge Pressure	0 – 50kPa
Tube Size	OD 2.5mm, ID 1.5mm
Tube Length	60mm on inlet and outlet (approximate)
Tube Material	Silicone
Motor	DC Geared Motor
Voltage	3VDC
Power Consumption	0.12W
Weight	11g

Figure B.1: Specification Sheet for the pump

Vita

Jack Worthington Stickley was born in St. Croix, USVI in 2001. After moving around, he called Knoxville home while attending the University of Tennessee to complete his Bachelor of Science in Aerospace Engineering. Prior to the start of his senior year, he joined a couple of other students to initiate the Aerospace and Defense Undergraduate experience (ADUE) to complete their senior year at UTSI. While under the guidance of Dr. Trevor Moeller, he got involved with the µSTAMPS project with the CEAR group. From here, he was accepted into the CEAR group as a graduate student where he pursued his Master of Science in Aerospace Engineering through work with the µSTAMPS project, as well as leading the new group of ADUE students to their success.